CONSTRUCTION OF MONOLITHIC ALL-GLASS OPTICAL CAVITIES FOR TRAPPING ULTRACOLD ATOMS

A Thesis

Submitted to the Faculty

in partial fulfillment of the requirements for the

degree of

Masters of Science

in

Physics

by

Jesse Evans

DARTMOUTH COLLEGE

Hanover, New Hampshire

March 23, 2017

Kevin C. Wright, Advisor

Alex J. Rimberg

Kristina A. Lynch

F. Jon Kull, Ph.D.
Dean of Graduate Studies

Abstract

This thesis reports a successful testing of a procedure for the construction of a high-finesse monolithic glass bowtie cavity using hydroxide catalysis bonding. The design of the cavity is optimized for use in optical dipole trapping of ultracold atoms. The all-glass design is especially suited for experiments that include rapidly changing magnetic field, such as those employing Feshbach resonances. These all-glass hydroxide catalysis bonded cavities are ultra-high vacuum compatible and survive moderate bake-out temperatures required to reach ultra low pressures.

We developed a set of alignment procedures and mechanical jigs for the purposes of precisely aligning a symmetric bowtie cavity. The alignment procedures and jigs guarantee a minimal degree of cavity twist and maximize overlap at the beam crossing point. A prototype cavity constructed using these procedures was measured to have a beam overlap within the tolerances necessary to generate an effective crossed beam dipole trap.

Contents

Chapter 1

Introduction

The ultimate goal of this project is to design an optical cavity that allows for power buildup in a crossed-beam dipole trap for lithium 6 and lithium 7, leading to evaporative cooling of the atoms to the point of quantum degeneracy. In the grand scheme of cold atom physics, quantum degenerate atom mixtures are the foundation upon which more cutting-edge physics relies. In the long run, our group seeks to create ring Bose-Einstein Condensates (BECs) and Fermi gases while exploring current topics in ultracold physics such as 1D superfluid rings, the BEC-BCS crossover [15], the Fulde–Ferrell-Larkin-Ovchinnikov state [13], and effective dynamic gauge fields [6]. Exploration of all these topics is impossible until we create a quantum degenerate sample.

On the road to quantum degeneracy, the atomic mixture is first cooled in a magneto-optical trap (MOT) inside an ultra-high vacuum (UHV) chamber. The next step is to capture the mixture in a crossed-beam dipole trap consisting of two red-detuned lasers. The intensity of the optical fields is adiabatically decreased, lowering the trapping potential and allowing more energetic atoms to escape and causing

the captured atoms to re-thermalize at lower temperatures. A strong magnetic field is applied to take advantage of the Feshbach resonance's ability to tune atom-atom interactions, giving us control over the thermalization rate of the ensemble. When the atoms reach critical temperatures at a high phase space density, they become quantum degenerate, either in the form of a BEC or a quantum degenerate Fermi gas.

The scope of my work did not include cooling to degeneracy or exploring interesting many-body physics states, but it is necessary to understand each step along the way and to keep the end goals in mind when designing the dipole trap. Atypical design constraints have forced us to eschew conventional construction techniques and develop techniques of our own to work within experimental limits. I will outline both the constraints and the benefits reaped by adhering to them in the rest of this chapter.

1.1 Motivation

1.1.1 Cooling and Trapping Li atoms in a MOT

Our group has successfully cooled both ^{7}Li and ^{6}Li to millikelvin temperatures in a 3D MOT. I have included a picture of the MOT chamber and images of trapped lithium 6 and 7 from our experiment in Fig. 1.1

A MOT consists of a quadrupole magnetic field and counter-propagating lasers with frequencies close to a strong optical transition of the atomic species that will be cooled. The lasers are red-detuned from the cooling transition, so that when the atoms are moving towards one of the laser beams the Doppler shift induced by their

Figure 1.1: Lithium 6 and 7 MOT. Top Right: Trapped lithium 6. Bottom Left: Image of trapped lithium 7. Background Layer: The MOT experimental chamber

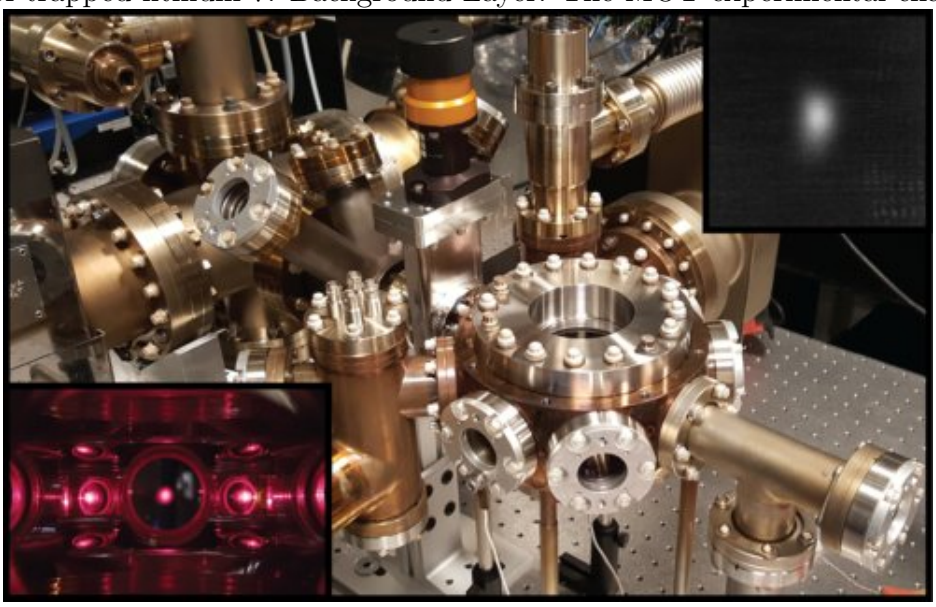

velocity causes the incident light to become resonant with the atoms, increasing the chances of absorbing a photon from the beam. The atom experiences a momentum kick of $\hbar k$ per photon absorbed, decreasing its average kinetic energy and resulting in "Doppler cooling". The quadrupole magnetic field has a minimum value (zero) at the center of the trap and an approximately linear positive field gradient in the local neighborhood of the zero. The field gradient results in a Zeeman shift of the hyperfine m_f sublevels of the atoms. Therefore, as the atoms move away from the field center their resonant frequencies shift closer to that of the detuned lasers, resulting in a restoring force that pushes them back to the center. A MOT with 3 sets of counter-propagating red-detuned lasers intersecting at right angles in a 3D quadrupole field, can trap atoms atoms along all 3 spatial direction and cool them to temperatures near the "Doppler limit" $T_D = \hbar\Gamma/2k_B$, where Γ is the linewidth of the transition, and k_B is Boltzmann's constant. For lithium, this temperature is well below 1 millikelvin.

In our setup, we made use of a 2D+ MOT and a 3D MOT to cool both ^{6}Li and ^{7}Li. In a UHV chamber we loaded both isotopes into the 2D+ MOT and applied counter-propagating red-detuned beams along the x and y directions, confining atoms along the z axis. We used a resonant "push beam" to propel the atoms along the z axis, creating a cold atom stream into the 3D MOT chamber. We then trapped the atoms from the stream in the center of the 3D MOT using 3 sets of orthogonal counter-propagating beams in a quadrupole magnetic field.

Laser cooling of alkali metal atoms usually employs light that is near-resonant with the $^2S \rightarrow ^2 P$ transitions, historically referred to as the Fraunhofer "D" lines. The fine structure interaction splits the ^2P electronic state into $^2P_{1/2}$ and $n^2P_{3/2}$. The transition from the ground state to the $n^2P_{3/2}$ (referred to as the D_2 transition) is the one typically used for laser cooling of alkali metals. All the alkali atoms have nonzero nuclear spin, and the hyperfine interaction splits the $^2S_{1/2}$ ground state in two as well. Two laser frequencies are therefore required for laser cooling, because if only one of the ground state manifolds is strongly coupled to the laser light, when the atoms undergo spontaneous emission from the excited state back to the ground state they may decay into the non-coupled manifold, and cease to interact with the cooling laser. The (stronger) transition coupling the upper hyperfine ground state to the excited state is conventionally called the "pump" transition, while the transition to the lower hyperfine ground state is called the "repump".

The specific transitions used for laser cooling of the lithium isotopes are shown in Fig. 1.2. To cool ^{7}Li, the pump and repump beams couple from the the $F = 2$ and $F = 1$ ground state manifolds (respectively) to the $^2P_3/2$ excited state. Similarly, for ^{6}Li the pump and repump beams couple from the $F = 3/2$ and $F = 1/2$ ground

Figure 1.2: Fine and hyperfine structure of the $^2S \rightarrow {}^2P$ transitions typically used in laser cooling of ^{6}Li (left) and ^{7}Li (right).

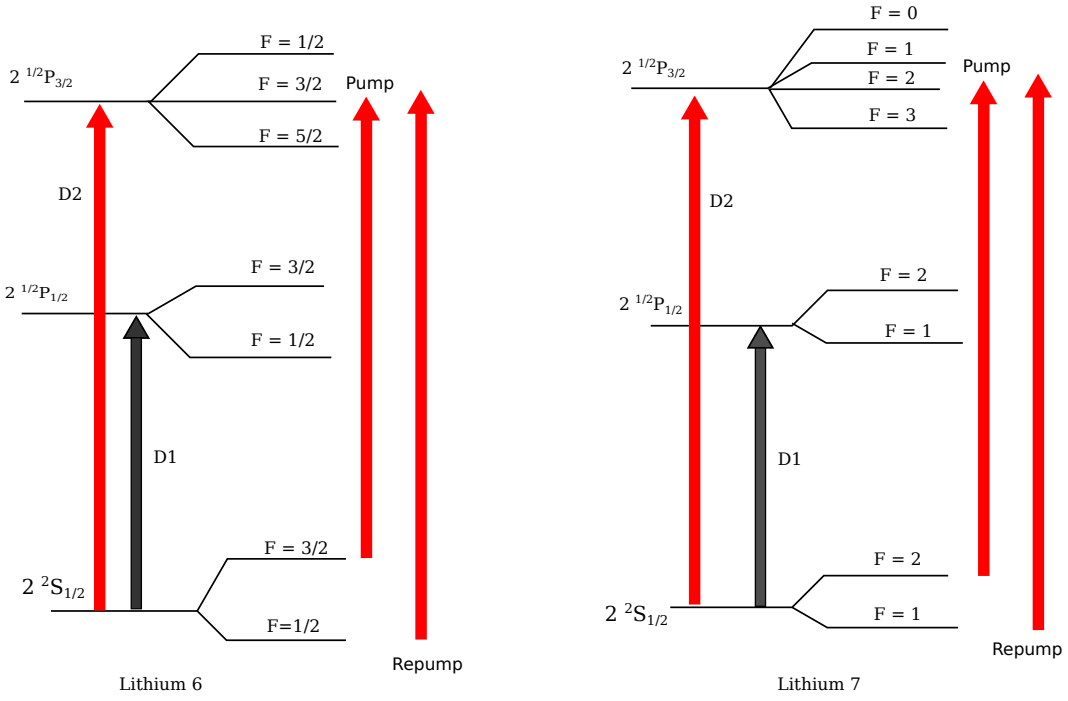

state manifolds to the $^2P_3/2$ excited states. In both lithium isotopes, the hyperfine splitting of the $^2P_3/2$ (D_2) excited states is smaller than the transition line width, and therefore unresolved.

Cooling and trapping the atoms in a MOT is the first step towards quantum degeneracy and dictates the starting conditions for the atoms we intend to trap in a crossed dipole beam setup. The starting atom numbers and temperatures for both species depend on the efficiency of the MOT. Other experiments have achieved MOTs with number densities of around 10^{10} cm^{-3} and temperatures below one mK [18], and we expect to be in the same neighborhood with our setup.

1.1.2 Crossed Dipole Beam Trap and Evaporation

Once our lithium atoms are cooled and trapped in a MOT, we need to cool them down to microkelvin temperatures to achieve high enough phase space density to reach quantum degeneracy. One of the more common ways to reach these low temperatures is to trap atoms in a crossed beam dipole trap and slowly lower the trapping confinement in a process known as forced evaporative cooling.

Optical Dipole Trapping

When light is incident on an atom, it induces an oscillating electric dipole moment on the atom given by

$$\vec{p} = \alpha \vec{E} \tag{1.1}$$

where α is the atomic polarizability and E is the electric field of the light wave. The potential of the dipole moment is given by

$$U = -\frac{1}{2\epsilon_0 c} Re(\alpha) I(r) \tag{1.2}$$

where I have substituted working with the intensity of the light field instead of the electric field. We can assume a Gaussian beam mode for the light field, whose spatial intensity distribution is

$$I(r) = I_0 \left(\frac{w_0}{w(z)} \right)^2 e^{-r^2/w(z)^2} \tag{1.3}$$

where $w(z)$ is the beam diameter at z and w_0 is the beam diameter at the waist, or when the beam diameter is smallest. Note that the beam comes to a focus at the waist, where the intensity decreases away from z = 0. The magnitude of the potential is therefore highest along the axis of the beam and at the beam waist. The sign of

the potential depends on the sign of the atomic polarizability, which is given by

$$\alpha = 6\pi\epsilon_0 c^3 \frac{\Gamma/\omega_0^2}{\omega_0^2 - \omega^2 - i(\omega^3/\omega_0^2)\Gamma} \tag{1.4}$$

for a given atomic transition at transition frequency ω_0, where Γ is the damping factor corresponding to the transition, given by

$$\Gamma = \frac{\omega_0^3}{3\pi\epsilon_0\hbar c^3} |\langle e|g\rangle|^2 \tag{1.5}$$

where $\langle e|$ and $\langle g|$ refer to ground (initial) and excited (final) states. Putting it all together, we finally have the general form for the potential, given by

$$U_{dip} = -\frac{3\pi c^2}{2\hbar\omega_0^3}\left(\frac{\Gamma}{\omega_0 - \omega} + \frac{\Gamma}{\omega_0 + \omega}\right) I(r) \tag{1.6}$$

The difference between the resonance frequency ω_0 and the laser frequency ω is generally referred to as the "detuning". The rate of photon scattering can be derived from the power loss, such that

$$\begin{aligned} \Gamma_{sc} &= \frac{P_{abs}}{\hbar\omega} \\ &= \frac{1}{\hbar\epsilon_0 c}\mathrm{Im}(\alpha) I(r) \\ &= \frac{3\pi c^2}{2\hbar\omega_0^3}\left(\frac{\omega}{\omega_0}\right)^3 \left(\frac{\Gamma}{\omega_0 - \omega} + \frac{\Gamma}{\omega_0 + \omega}\right)^2 I(r) \end{aligned} \tag{1.7}$$

Photon scattering involves the absorption and re-emission of a photon by an atom, and contributes to heating. Because the scattering rate is inversely proportional to the square of the detuning, whereas the trapping potential is inversely proportional to first order, we design our trapping wavelengths to be far from resonance to minimize

incidental heating. We detune far to the red (below resonance frequency) to make our trap high-field seeking, with a potential minimum at the focus of the beam. Note that trapping confinement is strongest along the radial direction of the laser, and weaker axially. To avoid the axial weakness, some experiments use a retro-reflected trapping beam that interferes with itself in a standing wave, creating a trap with a strong intensity gradient axially which results in a strong trap in 3 dimensions. However, the atom populations spread out across nodes spaced $\lambda/2$ apart, instead of a single potential minimum. We instead use a crossed beam configuration that has strong confinement along all 3 directions in the center of the trap. The crossed beam trap in a bowtie cavity can be configured to either have a standing wave potential or a traveling wave in the trapping region. I discuss these configurations in section 1.3.2. A more complete discussion of optical dipole trapping can be found in Ref. [10].

Evaporation and Feshbach Resonances

Feshbach Resonances The Feshbach resonance is a powerful tool that allows for the manipulation of the interaction strength within ensembles of ultracold atoms, using magnetic fields. Lithium is difficult to cool without using a Feshbach resonance, but the resonance is abnormally large in lithium, resulting in a much more realizable cooling process if the resonance is used [20]. The resonance is used to facilitate forced evaporative cooling and to tune the chemical potential of an ensemble as the atoms cool to degeneracy. In experiments that make use of metallic mounting schemes for optical cavities, the strong magnetic fields that induce the resonant effect can be distorted by the metallic mounts or induce forces on the mounting structure itself, resulting in a disruption of the cavity. We have avoided these risks by using an

all-glass optical cavity.

To understand the basic idea behind the Feshbach resonance, assume that there are two scattering channels for a pair of atoms in a scattering event, an energetically allowed, or "open", channel, and an energetically forbidden, or "closed", channel. In the classical regime the channels would not be coupled and the atoms would have a scattering length corresponding to being localized in one potential. In actuality, coupling between a closed and open channel can occur if the bound state of the closed channel and the background level of the open channel are near the same energetic level.

Take for example a pair of atoms in the triplet spin state approaching each other for a scattering event. If the triplet spin state potential at large interatomic distances is energetically close to a bound state of the singlet potential, a Feshbach resonance occurs and the atomic scattering length changes based on the strength of the resonance. A magnetic field can be used to shift the relative energy of the closed and open channels to tune the scattering length. In figure 1.3 I have included a figure that shows the open and closed channels during a scattering event.

Figure 1.3: Open and closed channels near a Feshbach resonance [5]

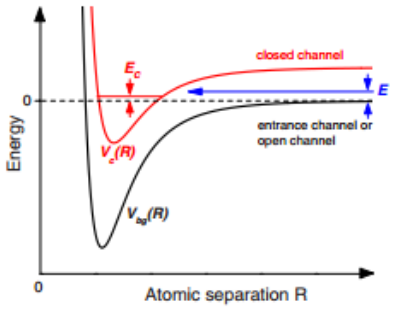

Forced Evaporative Cooling Evaporative cooling can be used to reduce the temperature of an atomic ensemble by first trapping the atoms in a potential well and then reducing the confinement of the trap adiabatically. As the trap's confinement is reduced, the most energetic atoms escape the trap and the atoms rethermalize at lower temperature. In our experiment we will use a crossed beam dipole trap in a cavity to confine the atoms and lower the optical power to decrease the trap confinement.

We will make use of the Feshbach resonance of lithium to facilitate rethermalization as atoms are released from the trap. If the rethermalization time is too long compared to the vacuum-limited lifetime of the atomic ensemble, it is not possible to increase the phase space density. If a Feshbach resonance is used, the scattering length is tuned to cause the atoms to interact and rethermalize on faster time scales, reducing opportunity for losses and maximizing phase space density.

1.2 Optical Cavities

1.2.1 Cavity Properties

In the simplest scenario, an optical cavity is a pair of mirrors facing each other [17]. Incident light is resonant with the cavity if the following condition is met:

$$d = \frac{q\lambda}{2} \tag{1.8}$$

where d is the length of the cavity, λ is the wavelength of the light, and q is an integer multiple known as the longitudinal mode order.

Figure 1.4: Linear cavity of length d

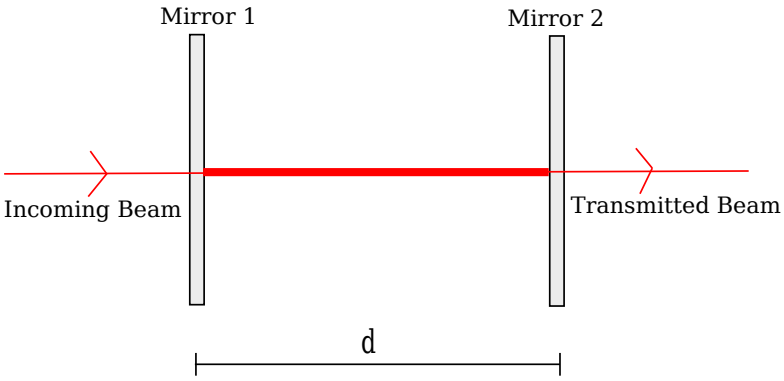

The separation between resonances in frequency space is known as the Free Spectral Range (FSR), given by

$$\nu_f = \frac{c}{2d} \tag{1.9}$$

where c is the speed of light. The admitted light is reflected within the cavity until transmitted through one of the mirrors (or scattered, or absorbed).

The cavity mirrors have inherent reflectivities, losses, and transmissions that describe how likely a photon will be lost, reflected, or transmitted through a mirror interface. Cavity resonances have a finite linewidth, taken as the full width at half max (FWHM). Finesse ($\mathcal{F}$) is a ratio of the FSR (ν_f) to the cavity linewidth ($\delta\nu_{cav}$) and is also a measure of the average number of reflections a photon will experience within the cavity, such that

$$\mathcal{F} = \frac{\nu_f}{\delta\nu_{cav}} \tag{1.10}$$

We now need to determine the finesse in terms of the amplitude of the field reflected from ($r = E_r/E_i$) and/or transmitted through ($t = E_t/E_i$) the cavity

Figure 1.5: Diagram of ray tracing in a bowtie cavity

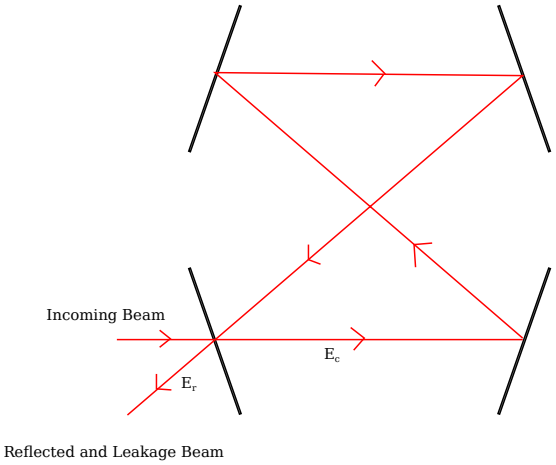

input mirror. The ring cavity we constructed is a 4 mirror symmetric bowtie (beams cross in the center at right angles, see figure 1.5). If the 4 mirrors have identical amplitude reflectivity, r, the relationship between the incident (E_i) intra-cavity (E_c), and reflected (E_r) field amplitudes is as follows:

$$E_c = tE_i + tr^4 E_c e^{ikL} \tag{1.11}$$

$$E_r = tr^3 E_c e^{ikL} - rE_i \tag{1.12}$$

Notice that outside the cavity, the light trickling out of the cavity interferes with the light reflected off the cavity mirror and that the cavity light picks up a phase shift as it travels within the cavity. Solving for the *power* reflection and transmission

coefficients of the cavity input coupler as ratios of field amplitudes yields the following:

$$R = \left|\frac{E_r}{E_i}\right|^2 = \frac{r^2}{1 + r^8 - 2r^4\cos(kL)} \tag{1.13}$$

$$T = \left|\frac{E_t}{E_i}\right|^2 = \frac{t^4}{1 + r^8 - 2r^4\cos(kL)} \tag{1.14}$$

The maximum amount of input power will be coupled into the cavity when R is minimum, *i.e.* when $\cos(kL) = -1$, such that

$$C = 1 - R_{min} = 1 - \frac{r^2}{(1 + r^4)^2} \tag{1.15}$$

In the limit that $r \to 1$ the maximum achievable coupling with 4 identical mirrors is 75%. However, it is also possible to use mirrors of different reflectivity, and maximize the coupling in a given configuration. This is referred to as "impedance matching" the cavity. For all the work in this thesis, we assume mirrors with identical reflectivity.

The denominators of equations 1.13 and 1.14 define the linewidth of the cavity through the coefficient of the cosine term. The denominators here are defined as F which is known as the coefficient of finesse. The linewidth (ν_{cav}) of the cavity is defined such that

$$k\frac{L}{2} = \pi\frac{L}{c}(\nu \pm \frac{\delta\nu_{cav}}{2}) = n\pi \pm \frac{1}{\sqrt{F}} \tag{1.16}$$

where n is some integer, and so combining we see that the finesse of a bowtie cavity is

$$\mathcal{F} = \frac{\pi r^2}{1 - r^4} \tag{1.17}$$

Extending the arguments above to the simpler configuration of a linear cavity, it can

be shown that the finesse of a linear cavity is

$$\mathcal{F} = \frac{\pi r}{1 - r^2} \tag{1.18}$$

The power buildup factor of a cavity is the ratio of intracavity power (P_c) to input beam power (P_i), given by

$$PBF = \frac{P_c}{P_i} = \frac{1 - r^2}{(1 - r^4)^2} \tag{1.19}$$

for a bowtie cavity. Thusfar I have assumed that all light incident on a mirror is either transmitted or reflected, such that

$$R + T = 1 \tag{1.20}$$

In actuality, some power is scattered or lost on any optical surface, so the above equation becomes

$$R + T + L = 1 \tag{1.21}$$

where L represents losses. Losses effectively reduce the reflectivity of the cavity, broadening the cavity linewidth and reducing power buildup, and reduce the coupling efficiency, particularly in the limit where the transmission and losses are of similar order.

1.2.2 Cavity Modes

Thus far I have treated optical fields as rays. In actuality they vary both longitudinally and transversely. The profile of the electric field of a laser is actually a solution to

the paraxial Helmholtz equation, and the form of such solutions is given by

$$E_{mn}(x,y,z) = E_0 \frac{w_0}{w} H_m\Big(\frac{\sqrt{2}x}{w}\Big) H_n\Big(\frac{\sqrt{2}y}{w}\Big) e^{-(x^2+y^2)(\frac{1}{w^2}+\frac{ik}{2R_c})-ikz-i(m+n+1)\zeta(z)} \tag{1.22}$$

where w is the spot size, w_0 is the beam waist, H_n are the Hermite polynomials, R_c is the radius of curvature, and ζ is the Guoy phase shift. The beam mode is characterized as the TEM_{mn} mode, where TEM stands for Transverse Electric Mode and m and n refer to the indices of the Hermite polynomials. Most lasers have a roughly Gaussian transverse intensity distribution, i.e. they are well approximated by the TEM_{00} mode. Inside an optical cavity, the beam mode is set by the path length, geometry, and mirror curvature. If the incident beam of the cavity is mode matched, meaning that the incident beam has the same spot size and radius of curvature as the TEM_{00} mode of the cavity at the boundary conditions of the cavity, then only the TEM_{00} mode will be coupled. In practice, beams can be multimode, where they are some superposition of Hermite Gauss modes.

Mode matching can be achieved by modifying the incident beam's radius of curvature and spot size with a set of lenses. I have included a detailed procedure for mode matching in Appendix B. If mode matching is ignored or calculated improperly, higher order modes are excited inside the cavity. Different spatial modes possess slightly different frequencies, and so when scanning through cavity resonances they will appear as separate resonances. When trying to lock to a resonance, you can only lock to one TEM mode at a time, so proper mode matching ensures maximum transmitted power efficiency.

Cavity modes shift by a frequency

$$\delta\nu = (n+m)\nu_f \frac{\zeta_g}{2\pi} \tag{1.23}$$

where ζ_g is the Gouy phase shift, a phase shift compared to a plane wave of the same frequency that occurs when a Gaussian beam propagates axially [9], given by

$$\zeta_g = \arctan(\frac{z}{z_r}) \tag{1.24}$$

I have included figure 1.6 to show the distinction between mode splitting and free spectral range in frequency space.

Figure 1.6: Mode spacing vs FSR

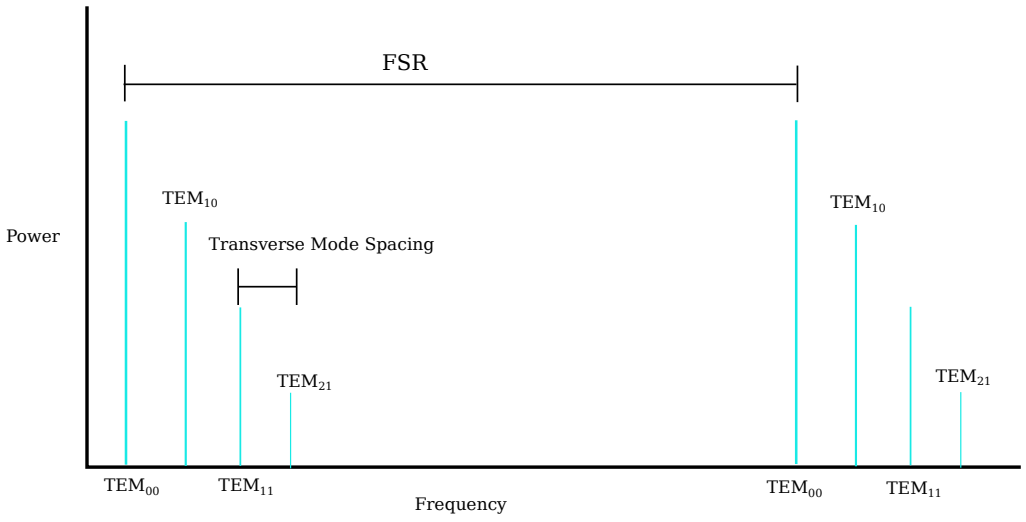

If a cavity mode is asymmetric (if beam has different spacial dimensions) or astigmatic (if the beam waist or curvature are different in different directions), the cavity

calculations, including mode frequency and mode matching conditions, must be done separately using the height and width of the mode independently.

1.2.3 Cavity Matrices and q Parameter

At any point along the beam axis, the transverse spot size can be given by

$$w(z) = w_0\sqrt{1 + \left(\frac{z}{z_0}\right)^2} \tag{1.25}$$

where z_0 is the Rayleigh length, given by

$$z_0 = \frac{\pi w_0^2}{\lambda} \tag{1.26}$$

The radius of curvature can be given by

$$R_c(z) = z\left(1 + \frac{z_0^2}{z^2}\right) \tag{1.27}$$

Both the spot size and radius of curvature are encoded into the q parameter, given by

$$\frac{1}{q(z)} = \frac{1}{R_c(z)} + i\frac{\lambda}{\pi w(z)^2} \tag{1.28}$$

While the q parameter initially seems like an awkward construction, it can be combined with ABCD matrix formulation to calculate the complex beam profile in complicated systems. ABCD matrices are numerical constructs that represent how

beam profiles change as they interact with optical elements, according to

$$\begin{bmatrix} q_2(z) \\ 1 \end{bmatrix} = k \begin{bmatrix} A & B \\ C & D \end{bmatrix} \begin{bmatrix} q_1(z) \\ 1 \end{bmatrix} \tag{1.29}$$

where q_1 and q_2 represent the q parameters before and after the element respectively and k is a normalization factor. ABCD matrices are well-known for many simple optical elements and can be looked up in a textbook [17]. The above matrix equation can be solved to give

$$q_2(z) = \frac{Aq_1(z) + B}{Cq_1(z) + D} \tag{1.30}$$

1.2.4 Cavity Locking

In an ideal world, lasers possess an infinitely narrow linewidth, never drift, and are noiseless. In the same ideal world, cavities have a perfectly fixed path length that is robust in the face of acoustic, mechanical, and thermal noise. Since the laboratory exists in the real world, we instead use electronic feedback to correct for noise and drift in both lasers and cavities [1].

General Locking Techniques At a very basic level, locking involves feeding instrument output to a locking device along with a desired setpoint that corrects any deviation from the setpoint. The locking device calculates an error value by taking the difference between the setpoint and the current output value and provides dynamic electronic feedback based on the error signal. As an example, consider a laser injected into a linear optical cavity whose output is monitored by a photodiode. The photodiode tracks the amplitude of cavity output and sends a voltage to a servo that

provides control feedback to the laser, such that as the laser drifts away from the set-point, the servo sends a signal to the laser controller that steers the laser frequency back towards the cavity resonance frequency.

One problem with this scheme is that if the laser is locked to the slope of a cavity resonance, due to the symmetry of the resonance a frequency shift across the resonance could cause the lock to be lost as it the signal slope switches from positive to negative, which would cause feedback in the wrong direction. Another issue is that amplitude fluctuations in the laser could falsely indicate a frequency shift from resonance. I discuss how we avoid these issues using the Pound Drever Hall method in section 2.5.

1.3 Experimental Design Constraints

Power Constraints

Typical modern optical dipole traps use lasers that produce hundreds of watts of optical power focused to a relatively small cross section to create a steep potential with which to trap atoms. Lasers that produce this much power are potentially dangerous and have relatively wide linewidths. They also cause thermal lensing effects on optics leading up to the chamber and on the chamber windows themselves, whereby the high intensity of the laser on the face of an optical element will impart enough thermal energy to warp the face of the optic slightly, distorting the beam over time. By contrast, using a less powerful but narrower-line laser in conjunction with a power buildup cavity presents an elegant solution to these problems.

Magnetic Constraints

The rapid switching of high magnetic fields necessary to tune the Feshbach resonance forced us to consider non-metallic mounting and construction options for the building of the cavity. Even non-ferromagnetic alloys of steel are more ferromagnetic than glass-type components, and the conductivity of metal allows for induction and eddy currents in the neighborhood of the center of the chamber, distorting the magnetic background. We therefore decided to attempt an "all glass" cavity, eschewing use of metallic construction materials.

Vacuum Constraints

Keeping our experiment chamber as clean and evacuated as possible is a high priority for our experiment. Our goal pressure for our main chamber is to sit at around 10^{-11} to 10^{-12} Torr, or roughly 15 orders of magnitude below atmospheric pressure. Given our goal to make our cavity all glass, vacuum constraints have ruled out use of conventional epoxies or resins, which out-gas too much to be used in experiments pushing the limits of ultra-high vacuum [11].

1.3.1 Trapping Atoms in Cavities

Experimental trapping of atoms in cavities has been performed since the beginning of the 21st century. In the following sections I outline some landmark experiments demonstrating atomic trapping in cavities to give our work some context and to show how our experiment differs from what has been done previously.

Linear Cavities

In 2001 Mosk et al. trapped spin mixtures of fermionic lithium atoms in a linear standing wave optical dipole trap at $\lambda = 1064$ nm in a glass cell [14]. The cavity mirrors themselves were placed outside of the cell and the cell windows were aligned to the cavity mirrors at the Brewster angle to minimize intra-cavity losses. The experiment took advantage of the Feshbach resonance of lithium to tune the interaction length of the atoms in the mixture. Their linear cavity achieved a finesse of about 600 and a power buildup factor of 130. They achieved a 0.8mK $\times k_b$ depth trap that held about 10^5 atoms after being supplied by a MOT with atom densities in the 10^{11} cm^{-3} range at $\leq$ 1mK. While they successfully trapped the atoms and avoided issues inherent in using metallic mounting in an experiment using magnetic fields to take advantage of a Feshbach resonance, they observed heating due to laser noise and losses on the cell walls, even at the Brester angle.

In 2010 Bruno Zimmerman and the Tillman Esslinger group out of ETH Zurich studied the microscopy of ultracold fermionic lithium while trapping atoms in a linear standing wave resonator [19]. This time the mirrors were mounted inside the vacuum chamber on metal pedestals. The cavity had a buildup factor of 6700 and a finesse of 10200, allowing the dipole trap to have a maximum trap depth of 48 μK$\times k_b$ at the location of the MOT where the dipole beam waist was as large as 760 μm. The cavity had very low losses resulting in high finesse and was able to successfully trap atoms, but a metallic mounting scheme would be unsuitable for our experiment that uses a Feshbach resonance. We would also like control over whether the trap was a standing wave or traveling wave trap, which is not provided in a linear cavity.

Ring and Bowtie Cavities

In 2003 Kruse et al. trapped ^{85}Rb atoms in a bidirectional standing wave trap in a 3-mirror cavity [12]. They explored momentum transfer between atoms and the cavity beams in both directions, noting that not only would photons redistribute themselves into the opposite direction beam after scattering off of the Rb atoms, but they would redistribute in between modes as well. Using p-polarized light they achieved a finesse of 2500 and using s-polarized they achieved a finesse of 170000. The high-q cavity produced 10W of intracavity power and had a trap depth of $k_b \times 1.4$mK using 799nm light. They used the Pound Drever Hall locking technique to lock to cavity resonances and were able to selectively couple to higher order modes and discussed the utility of higher order modes when evaporatively cooling to degeneracy. They were able to demonstrate 2-photon Raman transitions in a slowly moving standing wave trap, where an atom would periodically scatter from one Raman beam to the other and momentum would be imparted onto the atom. This cavity had high finesse using s-polarized light, but due to the lack of a crossed beam configuration the atoms ended up being stretched in the trap along the beam axis as opposed to localized at a point.

In 2011 Simon Bernon presented a high-finesse bowtie cavity for trapping and cooling rubidium and for performing non-demolition measurements on ensemble spin states [2]. The cavity mirrors were dual-coated for ultra-high reflectivity at 780 nm and high reflectivity at 1560 nm. They achieved a finesse of 1788 for 1560 nm light. Their mounting scheme was entirely metallic and adjustable either mechanically or with piezo-actuators. They used their cavity to measure spin states of atomic ensembles in a Mach-Zender interferometer, taking advantage of the high-Q capabilities of their cavity to provide generate high signal-to-noise detection while minimally dis-

turbing the system. This system was similar to the one we would design, but using Feshbach resonances for cooling Rb is not usually necessary, and so they made use of metallic mounting and alignment schemes unavailable to us.

1.3.2 Atom-Cavity Physics

While trapping in a cavity does solve some of the problems mentioned in section 1.3 inherent when using a high optical power laser, dipole traps without a cavity are actually cheaper and much easier to build. The trade-offs of using a lower power beam in conjunction with the cavity might or might not be worth the effort of complicating the overall experimental design. Another reason for using this scheme is that the field of atom-cavity interactions involves a lot of interesting physics in its own right, independent of the convenience of using the cavity for power buildup. By dual-coating the mirrors of the cavity for both off-resonant trapping frequencies (1068nm, in the IR) and on-resonant probing frequencies (671nm, in the red), the cavity can serve double duty for trapping power buildup and atomically resonant probing. I have outlined some examples of atom-cavity physics that would be possible to explore in the future using the results of this thesis.

Cavity Cooling Techniques

One advantage offered by using a cavity-based dipole trap is that it has been shown that you can use a slightly blue-detuned probe beam to reduce the kinetic energy and temperature of trapped atoms. Atoms in the beam path of the cavity act as a medium with a refractive index, changing the effective path length of the cavity. This change in path length results in an upshift of the resonance frequency of the cavity.

However, if the cavity has a high finesse, the off resonant photons do not immediately leak out of the cavity, resulting in a higher energy density in the beam. The system energy is conserved through inelastic scattering events with the atoms, resulting in a lowering of their kinetic energy and a drop in temperature. The cooling rate in some experiments was increased by a factor of up to 5 compared to more conventional means [16]. This method also has the advantage of being lossless, compared to the more standard evaporative cooling techniques in which losses are an inherent property of the system.

Quantum Non-Demolition Measurements

It is a basic tenet of quantum mechanics that performing a measurement on a system will change that system. Quantum non-demolition measurements are designed to indirectly measure the state of a system, resulting in a minimal impact on the system being studied. Cavities have been used in conjunction with Mach-Zehnder interferometers to make such measurements of the spin state of an atomic ensemble [2]. As I have stated above, atoms in resonant light act as a dispersive medium, which means they also induce a phase shift ϕ in the incoming light. If light makes N passes through the atoms, it experiences a phase shift of Nϕ. The phase shift depends on the state of the atoms, so if we have a mixture of atoms in a combination of two states, measuring the phase shift can give an indirect measurement of the atomic population ratio given a known total number of atoms. Groups have used this phenomenon in conjunction with high finesse cavities to create a large state-dependent phase shift in the cavity light and compare the phase shifted light to that of a local oscillator at the same frequency in a Mach-Zehnder interfermoter to measure the population

distribution of quantum gases in a non-destructive way [2].

Interference Control in Bowtie Cavities

Fine control of interference phenomena is inherent in a bowtie trap through manipulation of the polarization of the incoming beams. If the incoming beam is polarized in the plane of a cavity, at the center of the trap the crossed beams will have orthogonal polarizations, and no interference will be observed, creating a smooth trapping potential over the entirety of the overlapping region. If the beam is polarized perpendicular to the plane of the cavity, the polarization will be consistent throughout the cavity, and the crossed beams will interfere with each other, creating a 1-D interference pattern along the intersection of the beams. By adding a beam propagating in the opposite direction of the original beam, in the case of in-plane polarization a 2-D interference lattice pattern will emerge when the beams overlap in the center and a 1-D interference pattern will emerge in the case out-of-plane polarization.

Spontaneous Self-organization in an Optical Cavity

Spontaneous self-organization of atoms can occur in an optical cavity that possesses an empty cavity mode [7]. The self-organization can also be used to cool and trap the atoms further under the right conditions. Imagine an ensemble of atoms trapped in a standing wave trap that are being pumped by near-resonant light. There is a phase-position relationship in the trap, where a node is π out of phase with its neighboring node. Assuming a smooth distribution of atoms, scattering from atoms at one position in the standing wave are canceled out by the out-of-phase field contribution from its neighbor, resulting in complete destructive interference in the scattering field.

A uniform atomic ensemble will still have density fluctuations, however, resulting in a small scattered field with a random phase correlated to the density fluctuation. The scattered field will create a high field-seeking potential for the atoms (assuming that the field is red-detuned) which will tend to localize the initially uniformly distributed atoms. The shifted atoms will resonantly scatter photons in a preferred direction now in a superradiant mechanism similar to Bragg scattering, in which a lattice of atoms will act as a diffraction grating along a specific direction and will cause constructive interference of incident light along that axis. In the case of superradiance in a cavity, if the preferred scattering direction of the atomic ensemble is into a cavity mode, the effect will be self-perpetuating and result in a coherent shift of the atoms into potential wells corresponding to the newly populated cavity mode.

The coherent interaction between the atoms and the scattering field may result in a damping effect on the atoms due to the shift and broadening of the cavity resonances as the cavity field interacts with the atoms in a process similar to the one described in the Cavity Cooling section above, where kinetic energy from the atoms is lost into the shifting of the cavity modes. The damping results in atomic temperatures limited by cavity linewidth instead of the Doppler limit which is present in more orthodox atomic cooling mechanisms.

1.4 Cavity Construction Techniques

Optical cavities in vacuum are nothing new. An evacuated chamber provides a clean and noise-free environment ideal for narrow linewidth cavities. Cavity construction techniques in these environments vary based on constraints like space, cleanliness, and magnetic induction susceptibility. In the planning stage of this project we surveyed

a variety of construction schemes which I will describe in the following sections.

1.4.1 Standard Optomechanics

The most straightforward way of putting a cavity in a vacuum chamber uses metallic mirror mounts whose position and angle are governed by a set of either mechanical or piezoelectric actuators. Piezo devices expand or contract when supplied an electric voltage and allow for fine remote control of the mirror mounts. The leads of the piezo devices can be run through the side of the chamber which allows for instrument control outside the chamber [3]. The mirror mounts are bolted to a metal plate which is secured inside the vacuum chamber. Metallic mounting parts can have very low levels of outgassing. This scheme has the advantages of being highly vacuum compatible and allows for experimental adjustment in situ via the piezo actuators. It was deemed unsuitable for our experiment because the rapid switching of the Feschbach coils would create eddy currents in all conductive metallic alloys, disrupting the magnetic background uniformity in the experiment. The back electromotive force can also induce instability in the cavity itself. Many metallic alloys used for optomechanics are also ferromagnetic to at least a small degree, further distorting the background magnetic field in the chamber.

1.4.2 Monolithic Techniques

Monolithic optomechanics sacrifice adjustability for the sake of avoiding problems inherent in metallic mounting techniques. We surveyed a variety of possible bonding options before settling on one.

Epoxy

Some experiments avoid using metal components by using epoxy resins to fix glass components together to create a mounting scheme similar to the metallic one mentioned above. UHV-compatible epoxies are commercially available, but are only suitable in pressures 10^{-10} Torr or higher. Our experimental chamber must operate at lower pressures, between 10^{-11} and 10^{-12} Torr. We were also concerned that whatever outgassing occurred from the epoxies would increase absorption and scattering losses and decrease the finesse of the cavity to an unacceptable degree.

Optical Contacting

Optical contacting is a phenomenon whereby two surfaces that are flat on molecular scales and are extremely clean are bonded together purely by intermolecular forces when pressed together. This method has the advantages of being ultimately clean, involving only glass materials, and highly stable, but requires surfaces to be flat and clean to a difficult-to-attain degree. A more serious problem inherent in optical contacting is that the working time during the bonding is very low, and does not leave room for error when aligning the cavity. Given that we were trying to affix circular mirrors to flat mounts without obstructing or distorting any of the mirror faces, and that we would have a very short working window during the contacting phase while trying to align the cavity components, we deemed the method more trouble than it was worth when compared to the next option.

Hydroxide Catalysis Bonding

We ended up using a bonding method recently used in several high-precision applications such as LIGO and the LISA Pathfinder mission [8]. In hydroxide catalysis bonding, a small amount of bonding solution (sodium silicate in our experiment) is pipetted onto the interface of two flat, clean glass surfaces. The hydroxide solution dehydrates the silicate surface structures of the glass and causes them to bond together, leaving behind structurally rigid siloxane polymerized chains at the interface that holds the surfaces together as the water evaporates. Silicate mixed in allows for filling of gaps in the surfaces caused by surface mismatch or poor surface quality, making this method far more forgiving than optical contacting. If the surfaces are well matched, the bonding site is of optical quality.

Chapter 2

Development Process and Methods

2.1 Prior Work

Some first stage prototyping and testing was done by Sarah Khatry for this project. She put together a table-mounted bowtie cavity using 1" high reflectivity mirrors in a 1068nm beam line, observed the cavity resonances, helped develop the mathematical modeling code used for calculating beam parameters, and designed and assembled some of the locking setup. I have included a picture of the cavity setup in figure 2.1.

2.2 Hydroxide Catalysis Bonding Tests

One of the first experimental goals of this project was to determine the adaptability of hydroxide catalysis bonding (HCB) to UHV and high precision environments. To that end I performed a variety of tests to validate HCB for use in our experiment. Much of the currently existing literature suggests that a high degree of cleanliness, smoothness, and flatness is required of the elements to be bonded successfully. However this

Figure 2.1: Preliminary Bowtie

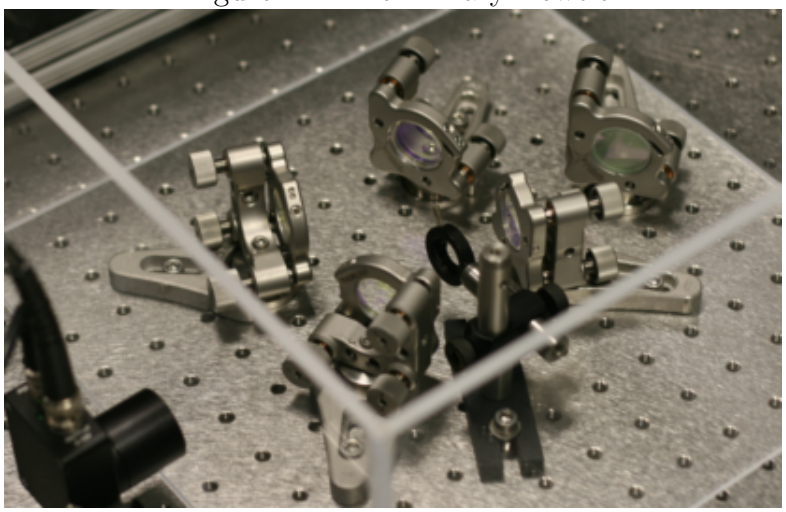

literature is centered around space-based astronomical applications like the LISA Pathfinder mission [8], and so bond strength in the face of being launched into space has a higher priority in the literature than it does in our experiment. We needed to determine if bonding curved and rough surfaces together was an option for our setup.

Preliminary Bonding Tests I bonded commercially available microscope slides to each other to determine how difficult it would be to bond non-ideal surfaces. These slides had been sitting in a dusty drawer for some time and were not ideal optical elements. I cleaned the slides in distilled water and immersed them in an ultrasonic bath of methanol for 20 minutes. I prepared a 4:1 by volume distilled water to sodium silicate solution and partially immersed a closed beaker containing the solution in an ultrasonic bath for 30 minutes. I then attempted to bond 4 pairs of slides to each other using 0.5, 1, 1.5, and 2 μL of bonding solution and left the bonds to cure for 4 days, after which checking just for the presence of a bond between non-ideal elements. All 4 samples bonded.

In the next test I bonded a curved, commercially fine-ground surface to a polished flat one. I stood a 1" diameter optical-quality mirror on edge and slid 2 right angle prisms underneath to fix the mirror in place and bonded along the lines of contact between the mirror and prisms, as per the diagram in figure 2.2. I cleaned the mirror

Figure 2.2: Mirror Bonded to Right Angle Prisms

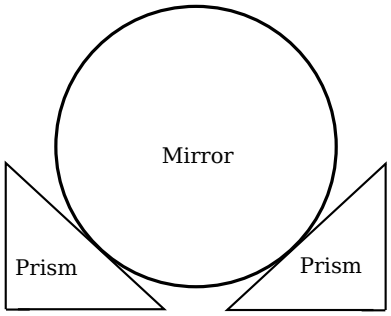

and prisms in distilled water and methanol and prepared a sample of bonding agent as described above. I used 2 μL of solution along the interfaces between the mirror and each of the prisms. After waiting to cure for 4 days, I determined once again that the bonding was successful, though it could be pulled apart by hand.

Bond Strength To put a quantitative measure on how strong the bond was using the hydroxide catalysis bonding procedure, I bonded smooth borosilicate glass spheres 0.5 cm in diameter to smooth glass microscope slides. Once the bonds were completed and allowed to cure, to determine bond strength for a given bond I fixed a wire to the top of the marble and hung a weight off of the other end of the wire, hanging off the edge of a desk. I have included a diagram of the setup in figure 2.3 and tabulated the resulting data in table 2.1.

Figure 2.3: Mirror Bonded to Right Angle Prisms

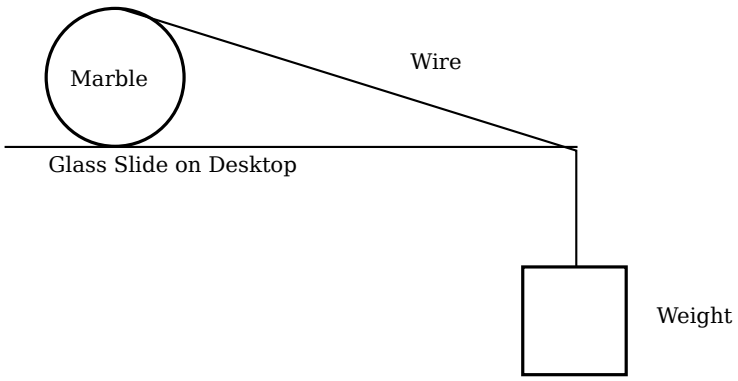

Table 2.1: Bond Strength Test Results

Volume (uL)	Breaking Weight for 4:1 Solution (N)	Breaking Weight for 3:1 Solution (N)
0.5	1.5	4
1	3	6
1.5	6	7
2	7	7

When testing the bond strength I hung progressively heavier weights off the edge of the desk until the bond broke, incrementing by 50g weights. We were concerned that using too much bonding agent in the experiment would result in water vapor outgassing in the chamber, so we tested both bond strength for different volumes of solution and bond strength for different solution concentrations.

We concluded that using 3:1 water to sodium silicate solution was more more likely to limit the outgassing load and provide better bond strength overall.

Cure Timing In the literature, bond strength was deemed to be maximized if the bond was left to cure for at least 4 days [8]. When we bonded two surfaces together throughout experiments, we used alignment jigs that might lack adequate long-term vibrational or mechanical stability, and so wanted to minimize the amount of time the optic spent curing while attached to the mount in case someone bumped a table or vibrations caused a bond to break. To that end, we wanted to ascertain how soon it was safe to remove optics from the mounting jigs and allow them to bear their own weight.

To do so, I set up a series of 1/2" mirrors bonded to microscope slides and allowed them to cure over different time periods, including a half hour, an hour, 2 hours, 4 hours, 12 hours, 24 hours, and 2 days. After the allotted curing times I would qualitatively determine the strength of the bond. I judged that after an hour or two, the bond could withstand at least minimal incidental force and could probably be removed from its mount safely. While this test was by no means quantitative, it provided us with a reasonable procedure to follow through the later experimental bonding stage, as we left the bonds to cure for 2 hours before removing the optics from their mounts but still waited 4 days before moving or touching the bonded optical assembly.

2.3 Bowtie Cavity Design

The bowtie cavity for use in the experiment must allow for certain design restrictions. It must fit inside the main chamber while accommodating the MOT beams. The mirrors must have a reflectivity and power buildup factor high enough to create a deep dipole trap, without having such a narrow linewidth that vibrations prevent

robust locking of the laser to the cavity. It must also allow access to both a beam reflection and transmission line through the chamber's viewports. Figure 2.4 shows a digital model of the entire vacuum chamber apparatus, including the 2D MOT cross, 3D MOT, and various pumps and gauges.

Figure 2.4: Complete Experimental System

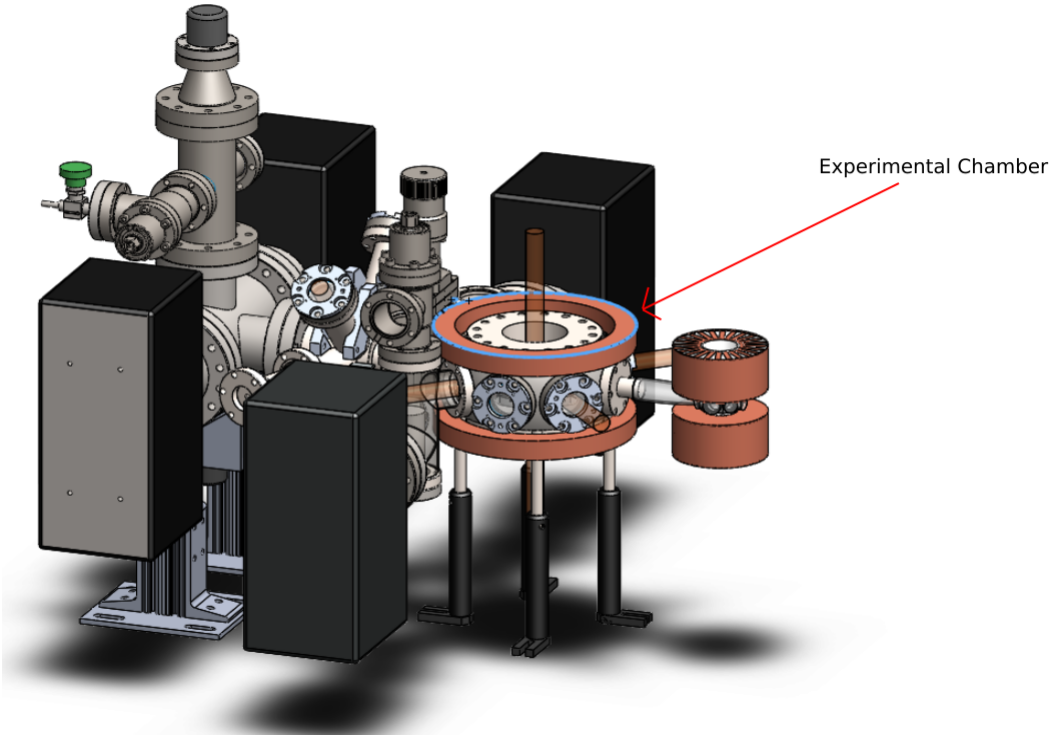

I have also included a model of the inside of the experimental chamber, including the cavity, MOT beams, viewports, and cavity beam lines. The red cylinders are the MOT beams and the black lines inside the cavity are the trapping beams. To accommodate the MOT beams, the cavity mirrors form a square 59 mm to a side.

In figures 2.6 and 2.7 I have included a model of the cavity itself. The mirrors are mounted on pairs of pentaprisms with a 5mm clear aperture, shown in Fig. 2.6. These 5-sided fused silica prisms happen to have an ideal height for mounting the

Figure 2.5: Experimental Chamber

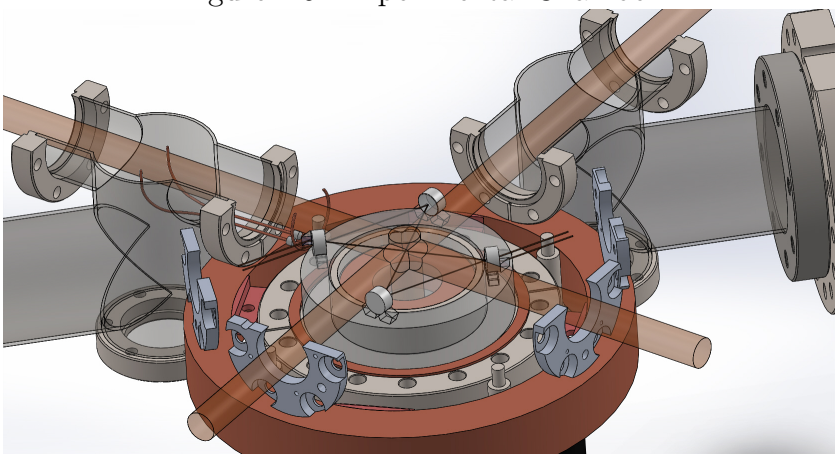

cavity mirrors 10.5 mm above the ring-shaped Zerodur spacer, as shown in Fig. 2.7. The whole assembly rests on four Viton rubber o-rings inside the chamber which help isolate it from acoustic excitations. The reflected beam exits the chamber at an angle that would cause it to clip on the viewports, so we have included in the design a right angle prism bonded to the back of the cavity mirror to redirect the beam outside the cavity so that it can be monitored.

Figure 2.6: Cavity Mirror Mounted on Pentaprisms

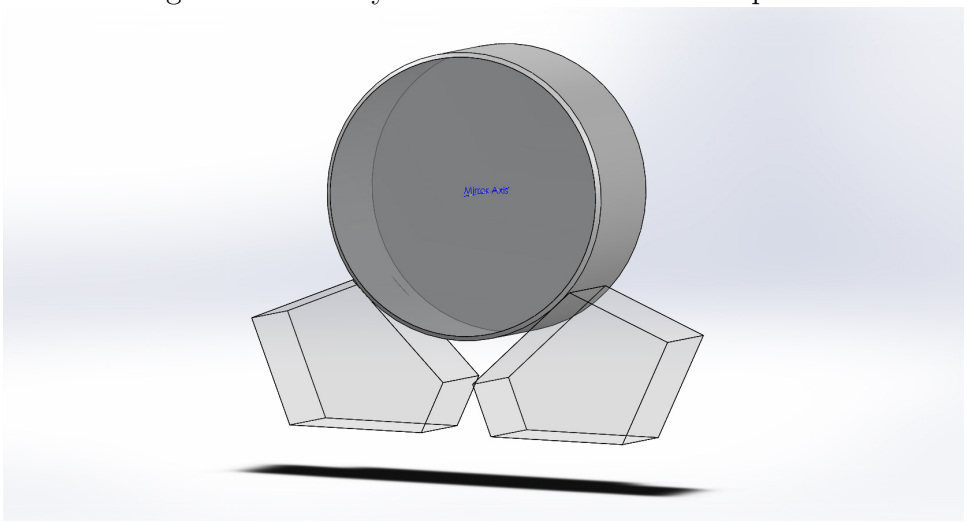

Figure 2.7: Model of Monolithic Bowtie Cavity for Experiment

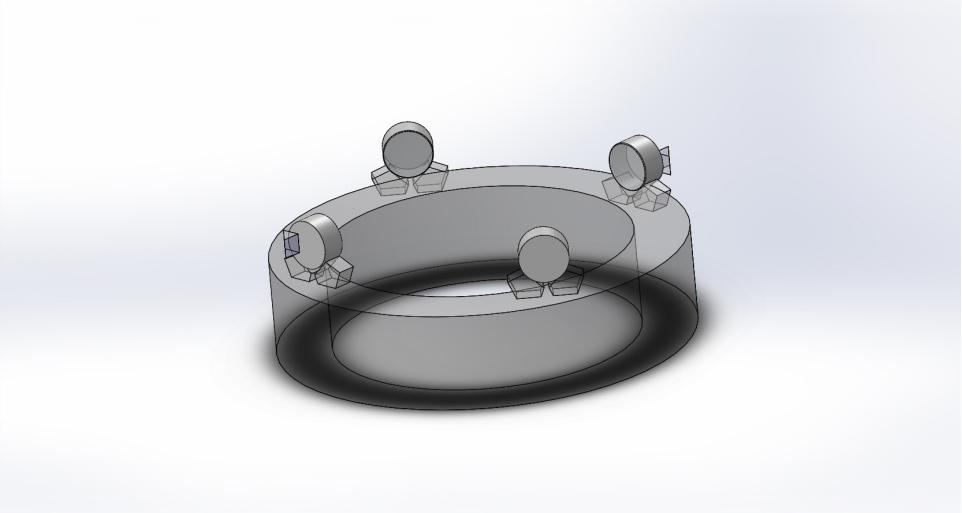

The mirrors themselves are high reflectivity and low loss. To improve coupling efficiency into the chamber, the input mirror is at a slightly lower reflectivity at $r \geq 99.98\%$ compared to the $r \geq 99.992\%$ reflectivity of the other mirrors. It is also important to note that the mirrors themselves are relatively far from the viewport windows, so mode matching schemes that require a lens within about 10 cm of the input mirror are impractical.

2.4 Modeling

Given the above design for the experimental bowtie cavity, we numerically modeled the dipole trap depth and shape following the arguments I made in 1.1.2. We also modeled how the power buildup factor would change based on mirror reflectivity, described in section 1.2.1.

Note that the power buildup is across all modes, so mode matching is necessary to assure that all the power resides in the TEM_{00} mode we use for trapping. I included

Figure 2.8: Power Buildup for Bowtie Cavity

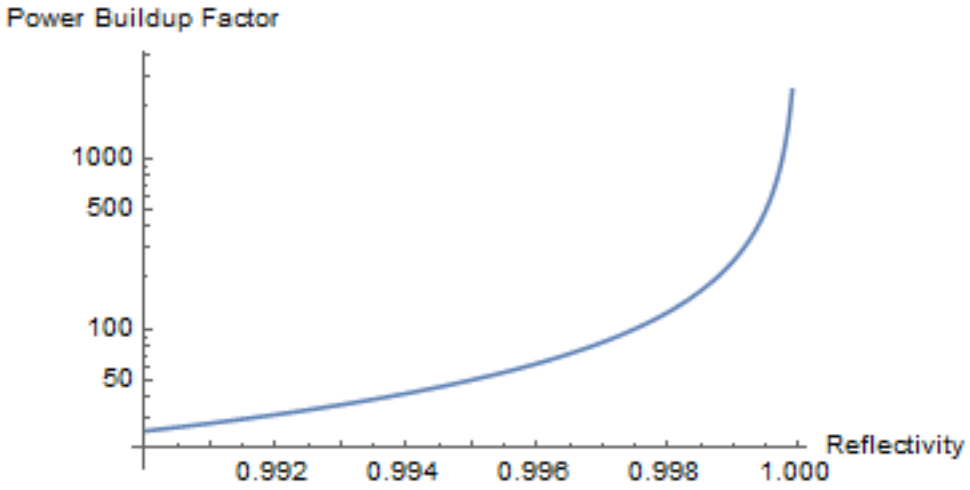

a graph of power buildup instead of just a number based on our mirror specs because the mirror specs are only given in terms of limits, so we do not have a precise quoted value for mirror reflectivities. Also note that the basic calculation of the power buildup factor does not take into account the input impedance of the cavity as described in **??**, so imperfect coupling could result in a lesser PBF. Assuming variable input power, the trap depth is 3.23 $\frac{\mu K}{W}$ of intracavity power and the harmonic trapping frequency of the trap is $492\times\sqrt{P}$ Hz where P is the intracavity power in Watts.The trap shape and depth are shown in figures 2.9 and 2.10, for an assumed intracavity power of 300 W.

2.5 Pound Drever Hall Locking

In section 1.2.4, I mentioned that a couple of the problems with basic locking techniques are that frequency and intensity fluctuations are indistinguishable and that shifting off resonance produces a symmetric decrease in amplitude, meaning that you

Figure 2.9: Dipole potential at the center of the cavity, in the plane of the cavity

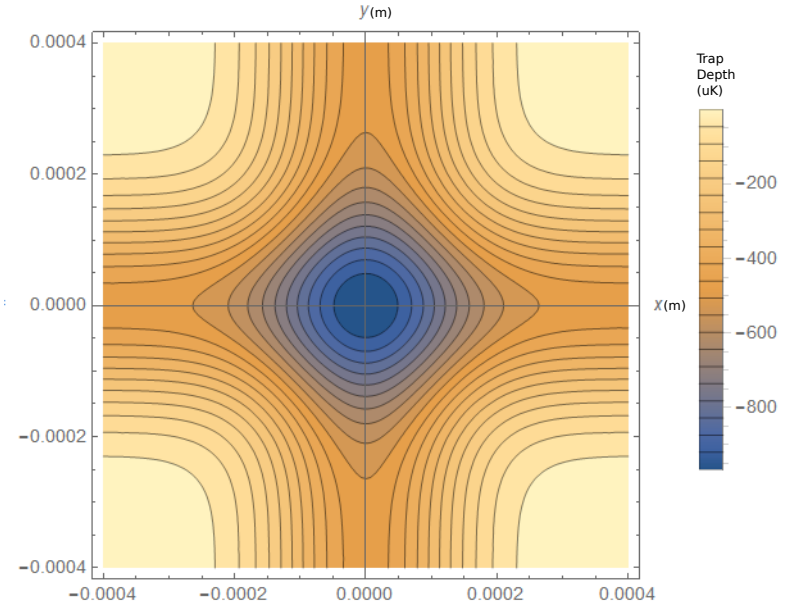

can not determine what side of the resonance you are on from the amplitude alone. The Pound Drever Hall locking method solves both above problems by looking at the derivative of the cavity resonance, which is anti-symmetric about the center, instead of the side of the resonance itself and by looking at the reflection off the cavity instead of the transmission line [4]. To make use of the derivative of the resonance, we put a sinusoidal frequency or phase modulation on the main line of the beam. If the frequency of the laser has drifted above that of the resonance, the modulation will be in phase with the intensity fluctuations resulting from moving in and out of resonance. If we are below the resonance, the frequency modulation and intensity fluctuations will be 180^0 out of phase. We can provide electronic feedback by comparing the phases of the intensity and the modulation, determining which side of the resonance we are on, and sending this information to a servo which provides feedback to the laser controller.

Figure 2.10: Dipole potential at the center of the cavity, perpendicular to the plane of the cavity, cutting along one of the beams.

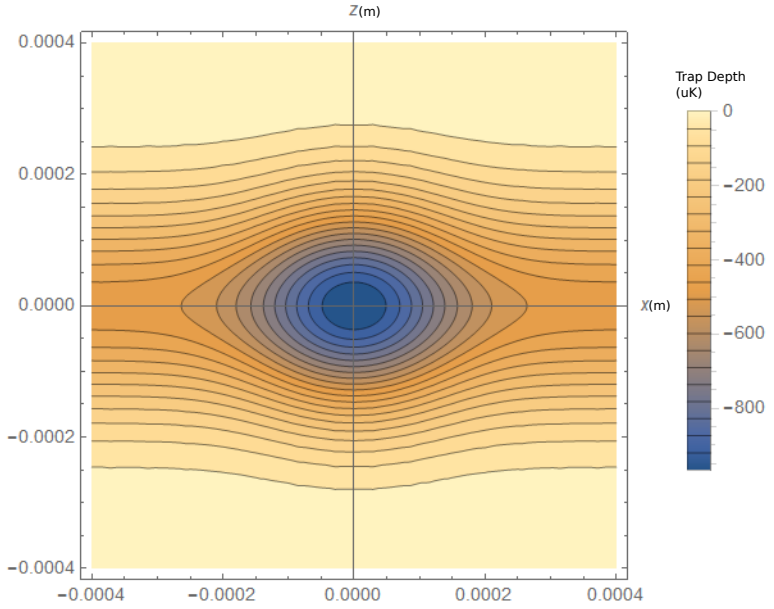

To mathematically model the error function produced using the Pound Drever Hall technique, let us assume that we have a lossless and symmetrical cavity. An incoming beam in the form

$$E = E_0 e^{i\omega t} \tag{2.1}$$

will have some portion reflected. We define the ratio

$$F(\omega) = \frac{E_{ref}}{E_{inc}} = \frac{re^{i\omega/FSR} - 1}{1 - r^2 e^{i\omega/FSR}} \tag{2.2}$$

as the ratio of the reflected and incoming beams' electric fields. Let us now put a phase modulation on the beam with modulation frequency Ω. The incoming beam

electric field becomes

$$E_{inc} = E_0 e^{i(\omega t + \beta sin(\Omega t))} \tag{2.3}$$

where β is the modulation depth. We can expand the above equation in terms of Bessel functions, giving

$$E_{inc} = E_0[J_0(\beta)e^{i\omega t} + J_1(\beta)e^{i(\omega+\Omega)t} - J_1(\beta)e^{i(\omega-\Omega)t}] \tag{2.4}$$

The above equation indicates that there are three beams to consider: one at the carrier frequency ω and then sidebands at $\omega \pm \Omega$. Here we assume that all the power is in the carrier frequency or the sidebands, and higher order modulations are ignored, which is reasonable for $\beta < 1$. The carrier and sidebands have powers

$$P_c = J_0^2(\beta)P_0 \tag{2.5}$$

and

$$P_s = J_1^2(\beta)P_0 \tag{2.6}$$

respectively. The reflected beam is similarly given by

$$E_{inc} = E_0[J_(\beta)0F(\omega)e^{i\omega t} + J_1(\beta)F(\omega+\Omega)e^{i(\omega+\Omega)t} - J_1(\beta)F(\omega-\Omega)e^{i(\omega-\Omega)t}] \tag{2.7}$$

The power at the detector from the reflected beam is

$$\begin{aligned} P_{ref} =& (\text{Constant terms}) \\ &+ 2\sqrt{P_c P_s}\,\mathrm{Re}[F(\omega)F^*(\omega+\Omega) - F^*(\omega)F(\omega-\Omega)]\cos(\Omega t) \\ &+ 2\sqrt{P_c P_s}\,\mathrm{Im}[F(\omega)F^*(\omega+\Omega) - F^*(\omega)F(\omega-\Omega)]\sin(\Omega t) \\ &+ O(2\Omega) \end{aligned} \tag{2.8}$$

Here I have neglected constant terms and 2Ω terms because when we multiply the signal at the detector with a local oscillator of frequency Ω using a frequency mixer, terms with different frequencies will go to 0 and not contribute. If we assume a fast modulation frequency and that we are close to resonance, the $\sin\Omega t$ term dominates, and mixing with a local oscillator supplying a $\sin(\Omega t)$ signal extracts an error signal of the form

$$\epsilon = 2\sqrt{P_c P_s}\,\mathrm{Im}[F(\omega)F^*(\omega+\Omega) - F^*(\omega)F(\omega-\Omega)] \tag{2.9}$$

The shape of the error signal is shown in Fig. 2.11. The error signal possesses a sharp, asymmetric curve centered at the resonance, providing a very convenient and unambiguous signal to lock to.

In figure 2.5 I have included a circuit diagram to show how we implemented PDH locking in our setup.

With the laser aligned to the cavity and scanning across cavity resonances, we modulated the frequency of the laser with an electro-optic modulator (EOM) (Thorlabs EO-PM-NR-C2) controlled with an amplified function generator signal. We used a half waveplate to rotate the beam polarization to allow full transmittance through the beamsplitter, then used a quarter waveplate to convert the beam polarization from

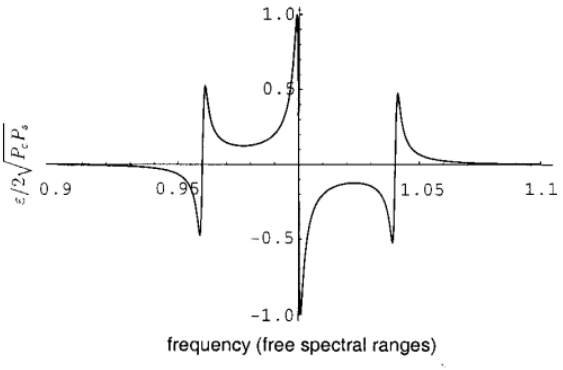

Figure 2.11: PDH Error Signal [4]

horizontal to circular. The beam reflected off the cavity is converted from circular to vertical and reflected off the beam splitter into the photodetector. The photodetector signal is high pass filtered to remove any DC offset and then mixed with the same function generator signal (now called the local oscillator signal) that was running the modulator. The mixer multiplies the signal from the cavity with the local oscillator.

The mixer outputs both a high frequency signal and a DC signal. We use a low pass filter to remove the high frequency portion. The DC component contains the phase-dependent differential signal derived above, which we then feed to a locking servo. We adjust the servo setpoint to the zero of the differential signal.

Figure 2.5 shows an oscilloscope trace of the error signal going in to the locking module of our laser, where the yellow trace is the cavity resonance on a photodiode and the blue is the error signal.

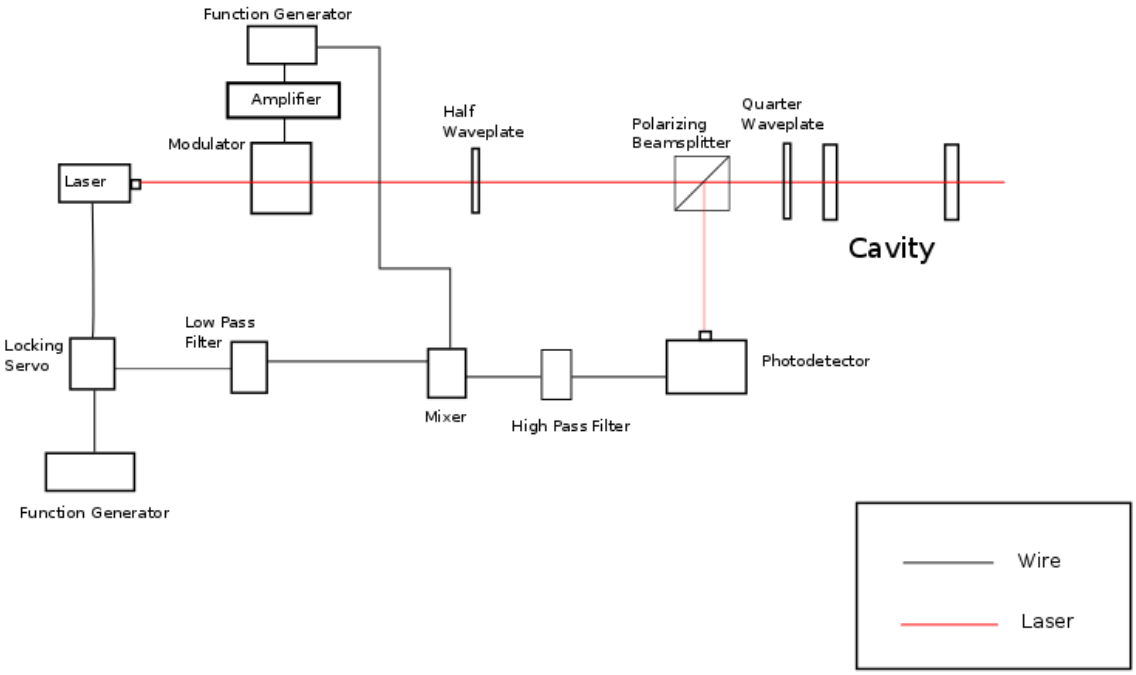

Figure 2.12: PDH Locking Setup

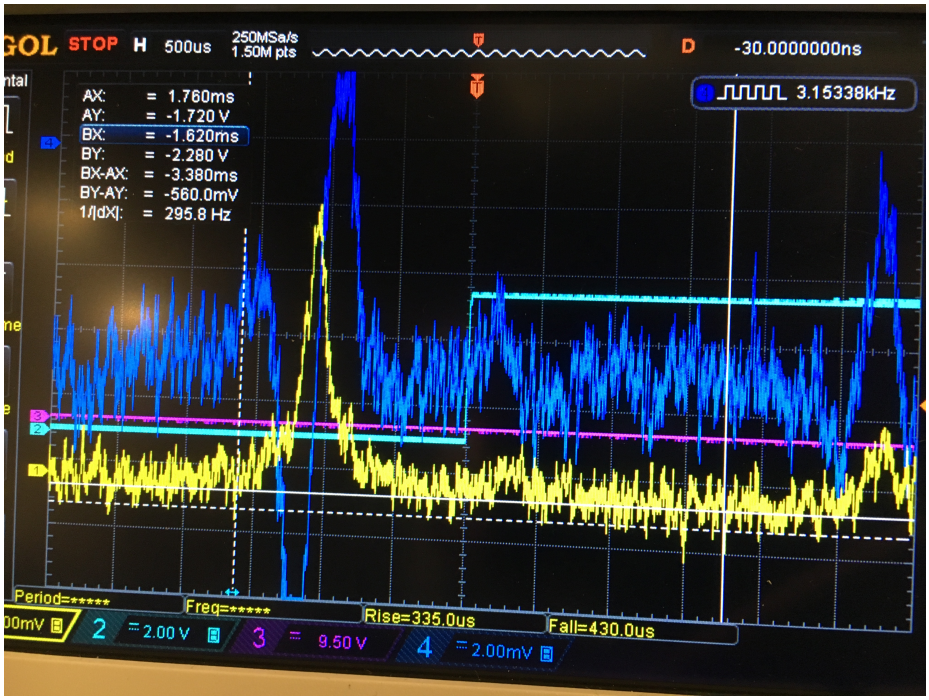

Figure 2.13: PDH Oscilloscope Traces. The yellow trace is the cavity transmission on a photodiode and the blue is the error signal generated from the beam reflected off the input coupling mirror.

Chapter 3

Results

Attempting to construct the experimental monolithic bowtie cavity using high quality but expensive materials seemed unwise without first testing out the individual components first. We wanted to ascertain whether or not hydroxide catalysis bonding a functioning cavity together would work on any level, to assemble and test the locking electronics setup, to check vacuum and bakeout compatibility of bonded cavities, to build up experience mode matching to cavities, and to develop a procedure for precision alignment of a bowtie cavity without using traditional mounting schemes, all before attempting to build the actual experimental cavity. The prototyping phase proved useful in guiding the development of our techniques and in increasing our likelihood of success when we actually attempt to build the experimental cavity.

3.1 Prototypes

3.1.1 Table-Mounted Linear Cavity 1

The first cavity we constructed simply consisted of 2 back-side polished mirrors coated for high reflectivity at 780 nm, held in place by "D" mirror mounts. I manually tested the mirror reflectivities by putting them in the laser line at normal incidence and comparing the transmitted power to the total laser power using a photodiode. The mirrors both had reflectivities of 99.17%. The measured reflectivities were low compared to that of the mirrors intended for use in the main chamber, but this feature was by design. The lower reflectivities allowed us to align the mirrors relatively quickly to verify our electronic PDH locking setup and alignment techniques.

The setup was identical to that described in section 2.5, with the exception that we modulated the beam frequency using a modulation input on the laser itself instead of an EOM. A photodiode was placed in the path of the transmitted beam and another in the path of the reflected beam coming off of a beamsplitter. A quarter waveplate was placed in the path of the beam just before the cavity to rotate the polarization of the reflected beam by a total of 90^0 so that the incident beam is transmitted through the beamsplitter but the beam reflected off the cavity was fully reflected through the same cube. The signal from photodiode measuring the transmitted beam was displayed on an osilloscope and the signal from the reflected beam was mixed with a local oscillator and used for feedback.

We placed an enclosure over the cavity with holes cut for the beams and floated the optical table on compressed air actuators to minimize mechanical and accoustic noise. To lock the laser to the cavity resonance, the resonance would have to have

drift in frequency space less than a linewidth away over short timescales. I measured the short and medium term jitter and drift of the cavity respectively. On a scan-to-scan time scale on the oscilloscope I measured that the resonance jittered by about a sixth of the linewidth. The cavity mode center was given to drift by about the same amount over a minute. While these measures were not particularly quantitative, they provided evidence that the noise would not prevent us from locking the laser to the cavity.

The laser was frequency modulated at 20 MHz and mixed with a local oscillator at the same frequency, resulting in a differential signal at corresponding resonance frequencies produced by the mixer. The differential signal was passed through a low-pass filter and fed into a locking servo which provided feedback to the laser. Using this scheme we successfully obtained a differential error signal and locked the laser to the cavity.

3.1.2 Monolithic Linear Cavity 1

I used the same mirrors from the 780 nm table-mounted cavity to construct a monolithic linear cavity prototype. I used a 2"x1"x1" borosilicate glass rectangular prism as the mounting surface. I fixed the prism to a 5-axis stage mount in the line of the 780 nm laser used in the table-mounted setup. I arranged the mirrors in mounting jigs fixed to the optical table using metal posts and right angle mounts. A picture of the jig setup is shown in figure 3.1. One of the mirrors was mounted in a 2-axis translation stage epoxied to a "D" mirror mount and the other was mounted on a kinematic stage similarly epoxied to a "D" mirror mount. I aligned the mirrors on the surface of the prism, relying on the kinematic and translation stages for align-

ment capabilities. I placed a photodiode in the transmitted beam line and aligned the cavity using the stages until I observed what I deemed to be optimal transmission resonances on an oscilloscope connected to the photodiode.

Figure 3.1: Jig Setup for Linear Monolithic Cavity 1

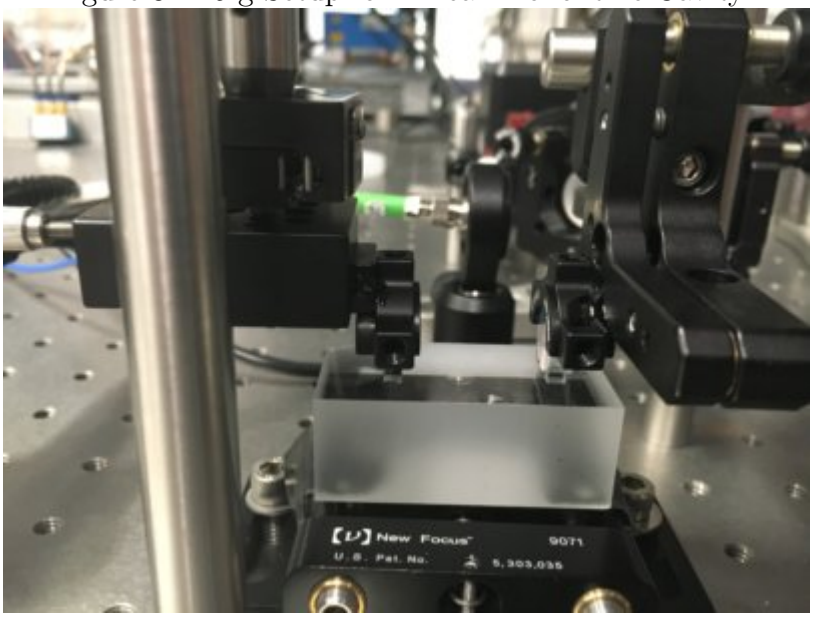

Once I deemed the cavity to be aligned, I used a micro manipulator tool to slide 3 mm right angle prisms bearing 1.5 μL sodium silicate solution into position under the curved edges of the mirrors to fix the mirrors in place. I then bonded the bases of the right angle prisms to the rectangular base prism and left the piece to cure for several days.

Once the cavity was bonded and the bonds cured, I aligned it in the 780 nm beam to determine whether or not the mirrors stayed aligned through the bonding process and to set a benchmark performance for comparison when I put the cavity in a vacuum chamber. The cavity stayed aligned enough to see strong resonances comparable to those before the bonding. I measured the cavity linewidth and FSR

by putting 26 MHz frequency sidebands on the cavity line as a frequency reference for the oscilloscope. By measuring the scope units corresponding to the sideband separation, I could establish a conversion rate between scope timing and absolute frequency while scanning.

I then measured both the medium and short-term noise on the cavity. Both the medium and long term drift and jitter were in line with what we observed in the table mounted linear cavity in that they shifted a fraction of a linewidth in each case as long as the cavity was covered to minimize noise due to air currents and acoustics. Once I had obtained reference performance data for the monolithic linear cavity, I constructed a vacuum chamber shown in figure 3.2 out of standard stainless steel vacuum parts.

Figure 3.2: Vacuum Chamber for Linear Monolithic Cavities

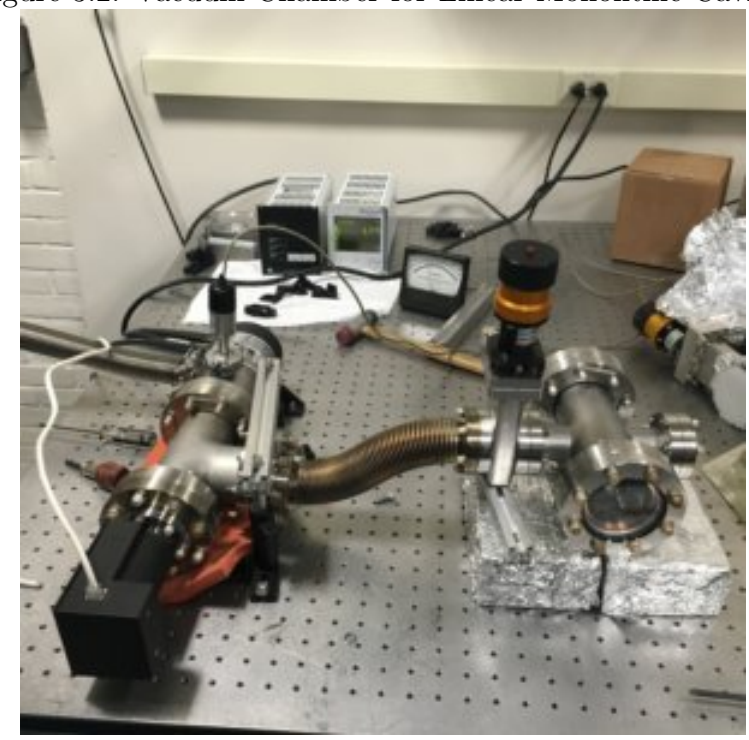

Table 3.1: Monolithic Linear Cavity 1

Test	FSR (GHz)	Linewidth (MHz)	Finesse	Mode Spacing (MHz)
Post-Bonding	6.9 ±0.13	14.6 ±0.3	471 ±9	160 ±3
In vacuum	6.9 ±0.13	35.6 ±0.7	193 ±4	166 ±3
Post Bake	6.9 ±0.13	35.0±0.7	196 ±4	163 ±3

I sealed the cavity inside the vacuum chamber, aligned the 780 nm laser through the cavity and vacuum chamber, and pumped the chamber down using a turbo pump backed by a roughing pump. Once the cavity was pumped down to minimum pressure at 5.8×10^{-9} Torr, I observed the FSR, linewidth, and mode spacing the same way as mentioned above. I then wrapped the chamber in silicon heating strips and slowly baked the cavity from room temperature to 125^0 C over the course of 24 hours to determine if the cavity could withstand the baking process we were likely to use in our main experiment. Once the chamber had been at 125 ^{0} C for about 12 hours, I slowly decreased the temperature of the chamber back to room temperature and retook cavity linewidth, FSR, and mode spacing measurements. All of the parameters measured post-bonding, in vacuum, and post bakeout are given in Table 3.1.

3.1.3 Monolithic Linear Cavity 2

We bonded together a second linear cavity to build upon our results from the first. Some key changes we made were that we used mirrors with higher reflectivity, mounted the mirrors on top of dove prisms bonded to a BK7 rectangular prism, and increased the length of the cavity to better model the longer length of the bowtie we were likely to build for experiment. The higher mirror reflectivity and increased cavity length increased the difficulty we faced in alignment and mode matching, simulating the

challenges we were likely to face when building the experimental bowtie. We also ground flats onto the bottom edges of the mirrors in lieu of using right angle prisms to hold them in place to determine the viability of a simpler mounting scheme. The mirrors were 99.97% reflective to perpendicular incidence of 780 nm light. While the cavity did eventually bond, bonding along the bottom flat of the mirror took a few attempts and overall seemed less robust than the right angle prism method.

I used ray matrix formalism to numerically calculate mode matching conditions for the cavity. I matched the collimated laser mode output from an optical fiber (350μ m waist) to the cavity mode using a 150 mm lens and a 50 mm lens in a Galilean telescope where the lenses were placed 200 mm apart and the 50 mm lens was placed 2 cm from the input cavity mirror. A more detailed description of mode matching is included in Appendix B. Using this scheme I managed to get about 95% of the intracavity power into the TEM_{00} mode, determined by sweeping through a full FSR and measuring the amplitude of each resonance. I verified that the coupled mode was TEM_{00} using a camera positioned on the other side of the cavity. An image of the mode is shown in figure 3.3.The other mode with observable population was higher order, shown in figure 3.4

Figure 3.3: TEM_{00} mode transmitted through the cavity

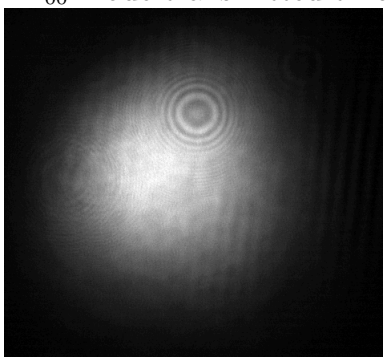

Figure 3.4: Higher Order Mode on Camera

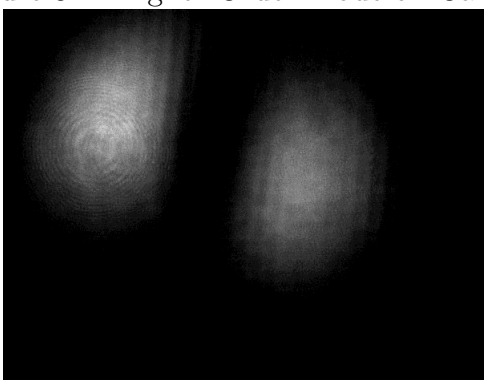

Table 3.2: Monolithic Linear Cavity 2

FSR (GHz)	Linewidth (MHz)	Finesse
1.82 ±0.03	5.7 ±0.1	316±6

This cavity had noticeably lower transmission throughput compared to the first monolithic linear cavity. I measured the reflected beam with a photodetector and observed that the TEM_{00} resonance dip was only 9% of the total reflected beam amplitude. In a cavity with no losses, resonant and mode matched light should be transmitted and completely interfere with the reflected light, so our 9% figure indicates that our cavity had high losses from some source, potentially the mirror coating which was not specified to have low loss compared to the transmission coefficient.

3.1.4 Table-Mounted Bowtie

As a precursor to attempting to bond a monolithic bowtie prototype we built a table-mounted bowtie cavity. The mirror separations were similar to those to be used in the experiment. The positions were set by using an aluminum plate with holes drilled at the correct positions to fix the mirrors mounts to, as shown in Figure 3.5.

Figure 3.5: Table-Mounted Bowtie Cavity

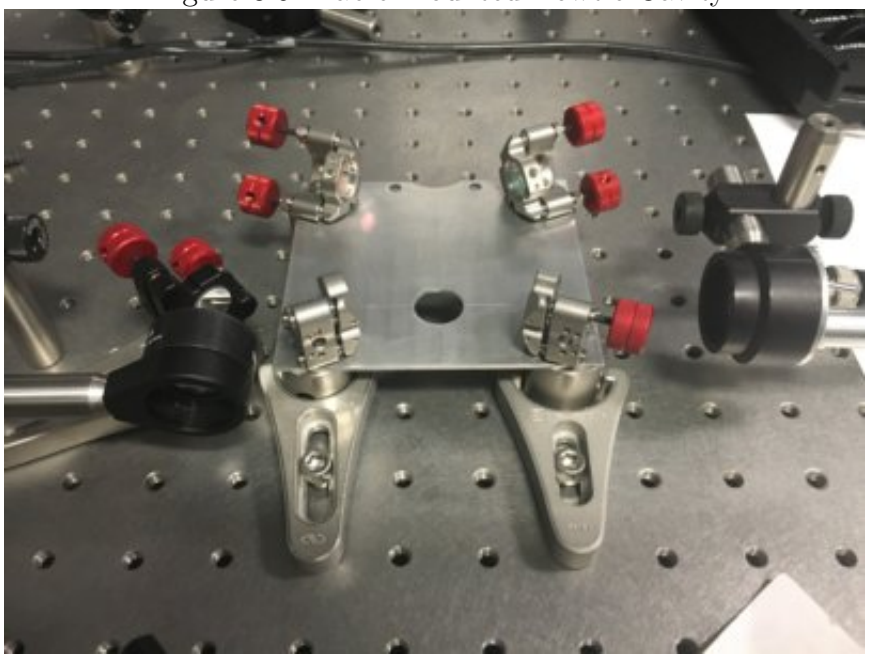

Table 3.3: Table-Mounted Bowtie

Polarization	FSR (GHz)	Linewidth (MHz)	Finesse
Horizontal	1.05 ±0.02	5.05 ±0.1	208 ±4

I used the paraxial ray matrix formalism to determine that a 100 mm and 50 mm lens pair in a Galilean telescope would match the collimated 280 μm waist input beam mode to that of the cavity (procedure described in Appendix B). After mode matching, about 96% of the intracavity power was in the TEM_{00} mode. I measured the FSR, linewidth, and finesse using a photodetector in a manner identical to how I have above with one exception. I attempted to measure the parameters for both horizontally and vertically polarized light. Cavity losses were so much greater with vertically polarized light that there was not enough signal to noise to take measurements.

3.1.5 Table-Mounted Linear Cavity 2

I aligned two of the high reflectivity, low loss Layertec mirrors to be used in the experimental bowtie in a linear cavity to determine their properties. We did not have time to fully analyze this cavity, but being concerned with our apparently relatively lossy mirrors, we wanted to test our low loss mirrors to verify that we were not making some systematic mistake with our cavity construction techniques. The cavity was aligned in a 1068 nm laser beam, frequency modulated at 1 MHz with an electro-optical modulator. A photodiode measured the light transmitted through the cavity.

I immediately observed that while there was visible scatter off of the face of the Thorlabs mirrors when viewed in the infrared, when the Layertec mirrors were illuminated with 500 mW of 1068 mn light and observed through an infrared viewer there was no detectable scatter. This was a good indicator of their low loss characteristics and cleanliness. I then measured the linewidth and FSR, and calculated the finesse of the cavity, as shown in Table 3.4.

Table 3.4: Table Mounted Linear Cavity 2

FSR (GHz)	Linewidth (kHz)	Finesse
1.01±0.02	250 ±5	4000 ±24

Using equation 1.18, I determined that with a measured of finesse of 4000, our effective reflectivity for the cavity mirrors was 99.961%. The quoted reflectivity was 99.97%. We found this result encouraging in that even if our prototyping mirrors were not ideal, our mirrors for use in the experiment would be.

3.2 Monolithic Bowtie Cavity

The final proof of principle for the experimental bowtie cavity was a monolithic cavity that matched the design parameters and restrictions in our experiment. The prototype was a square cavity 59 cm on a side. We bonded the four Thorlabs mirrors from the table-mounted bowtie on top of pentaprism pair supports that were bonded to a borosilicate glass substrate. I have included pictures of the resulting cavity and of the pentaprism support scheme in figures 3.6 and 3.7. The pentaprisms both serve to more securely bond the mirrors than the flat substrate surface would alone and to put the mirrors at the height planned for the experimental cavity in the experimental chamber.

Figure 3.6: Monolithic Bowtie Cavity

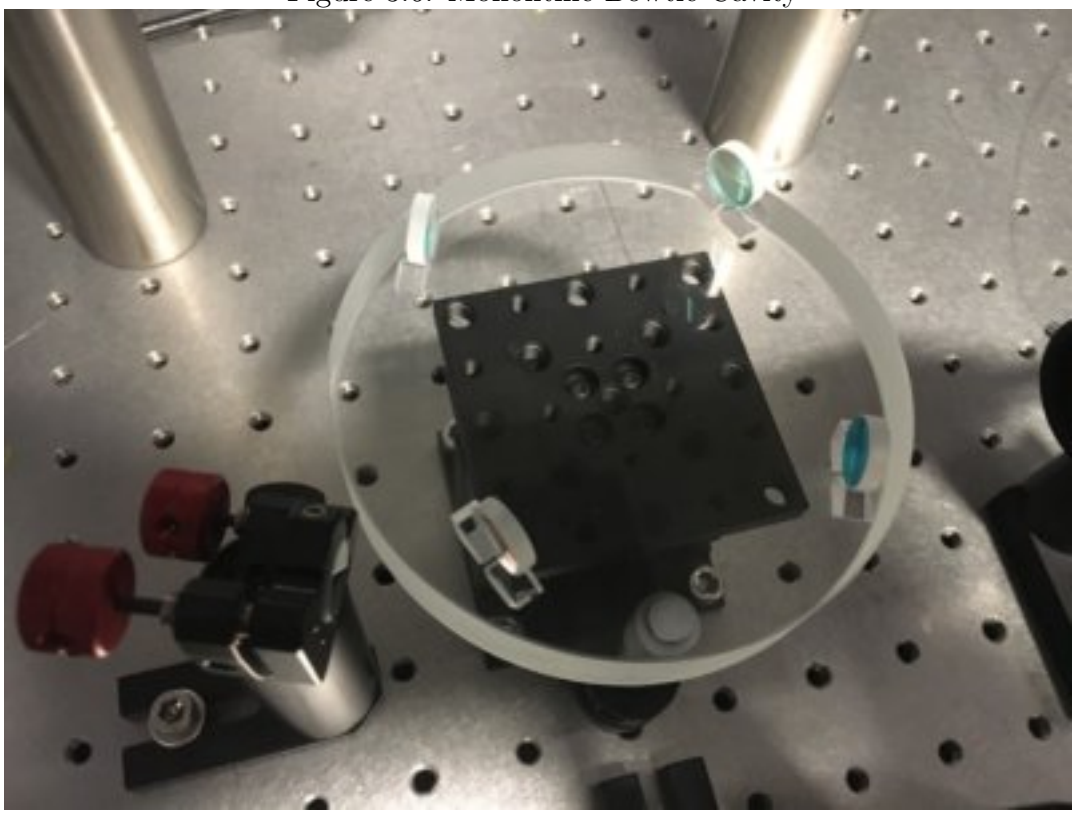

Figure 3.7: Mirror Supported by Pentaprisms

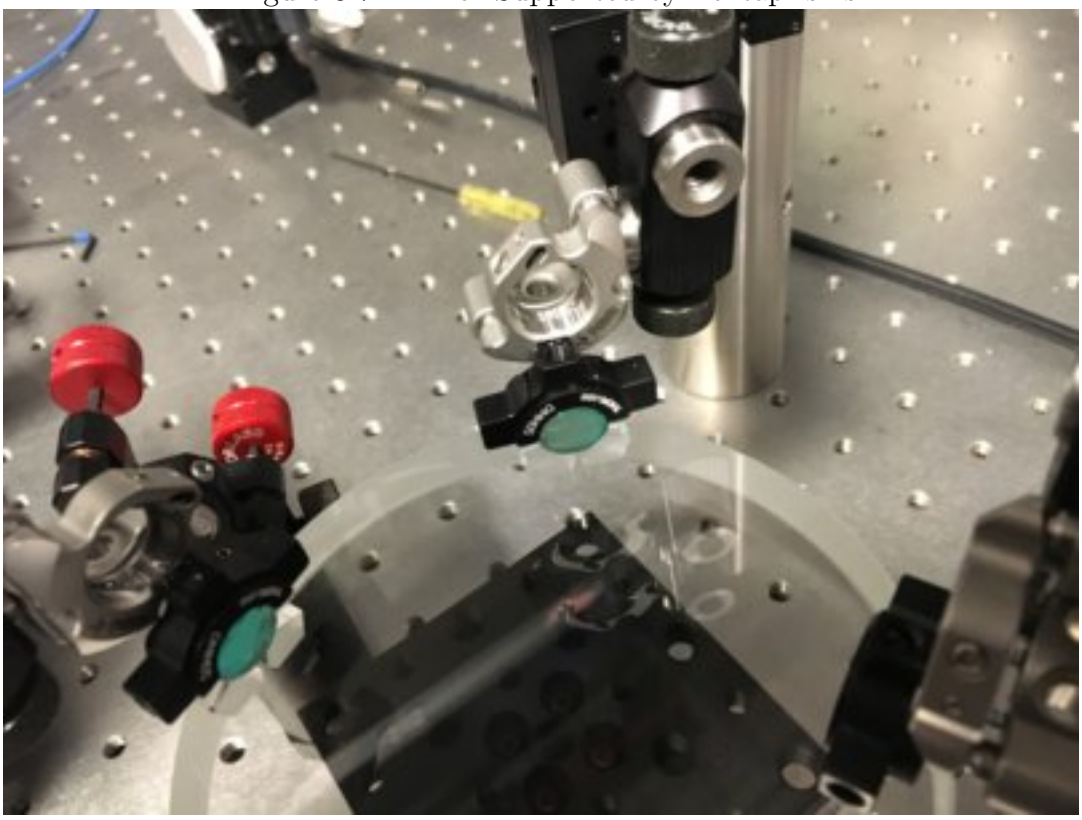

3.2.1 Jig Design

To make sure that the diagonal arms of the cavity overlapped in the center we paid particularly close attention to making sure there was no "twist" of the cavity mirrors our of the alignment plane, such that cavity modes were centered on each mirror and the mirrors were all in the same plane. To obtain precise positioning and angular fidelity in the construction process, we designed and had machined a metal jig that would set mirror locations and angles within narrow tolerances. I have shown a design and picture of the jig in figures 3.8 and 3.9.

The mirrors are fixed in "D" mirror mounts and placed into grooves in the jig. The inner entrance to each of the four grooves corresponds to the exact placement

Figure 3.8: Bowtie Cavity Alignment Jig Schematic

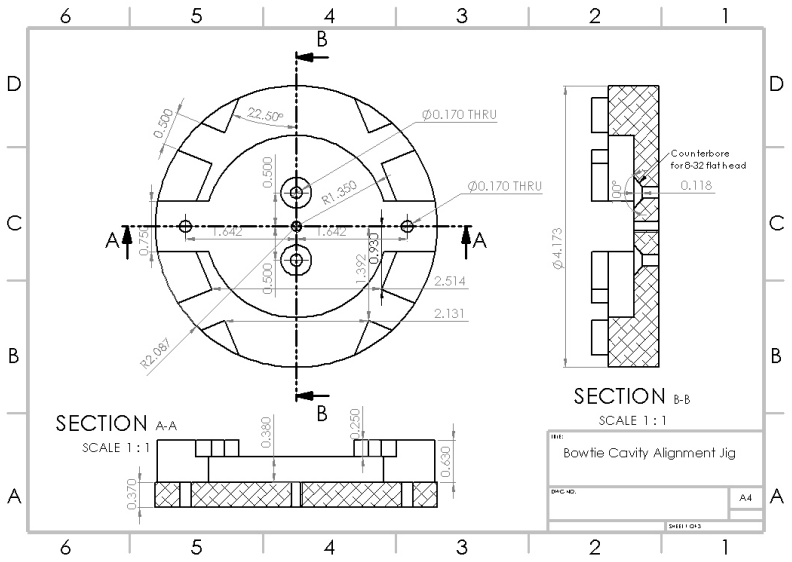

and angle of the mirrors in the cavity design. The mirrors are pressed against a flat precision gauge acting as a stop at the designed location and angle. The jig is screwed into a vertical translation stage to control the height of the cavity. We also had built a removable cylindrical insert piece for the jig with 280 μm diameter holes along the cavity beam line to act as a reference or guide during alignment.The jig was designed to be of similar height to our substrate so that once the mirrors were properly aligned in the jig, the stage could be lowered and the jig swapped out for the substrate. Shown in figure 3.10 is a rendering of the jig with the insert and options for fiber optic and pellicle alignment tools we decided not to use. The stage would then be raised again to appropriate height to accommodate the pentaprisms in the bonding process.

Figure 3.9: Bowtie Cavity Alignment Jig Model

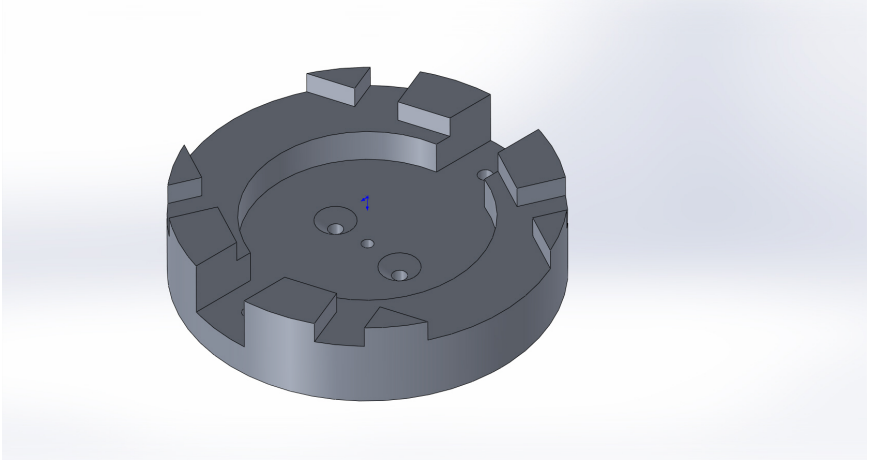

Figure 3.10: Bowtie Jig with Insert on Vertical Translation Stage

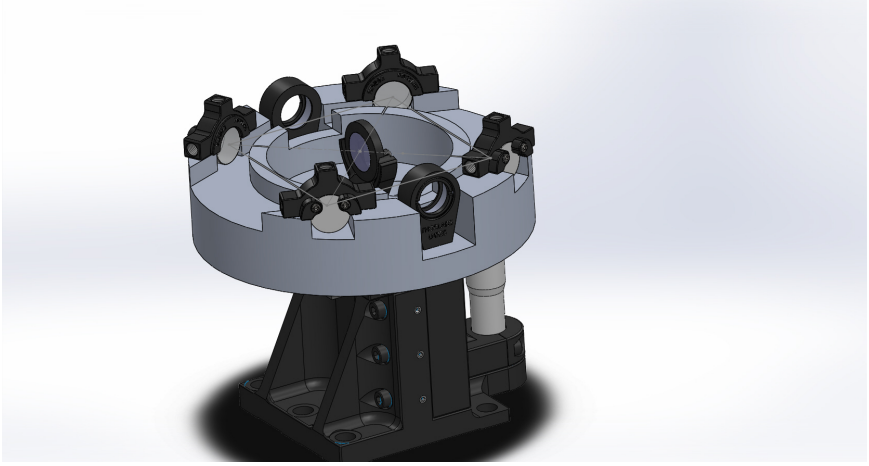

The jig itself allowed for initial alignment, but for fine alignment we set up mounts that allowed for vertical and horizontal tilt and for vertical and horizontal translation to maximize our control of the mirror locations. The mounting scheme used a Thorlabs Polaris mirror mount epoxied to the "D" mirror mount for tilt control and two translation stages fixed to the Polaris mount for translational control. The mounts were supported by 1" diameter steel rods fixed to the optical table.

3.2.2 Alignment Procedure

We aligned a 780 nm beam to the jig setup prior to inserting the mirrors into the jig. After the beam was roughly aligned to the first arm of the grooved guides in the cylindrical insert, we placed the mirrors in "D" mirror mounts into the jig and placed a photodiode in the transmitted beam line outside of the cavity. Due to refraction, the beam line shifted as it was transmitted through the first cavity mirror, so we adjusted to realign the beam to the guide. Once the mirrors were all in place and referenced to the jig using the precision gauge as a stop, we brought the mounting arms into contact with the "D" mirror mounts and epoxied the mounts to the mounting arms. I have included an image of the setup in Figure 3.11.

Figure 3.11: Mounting Setup (Top View)

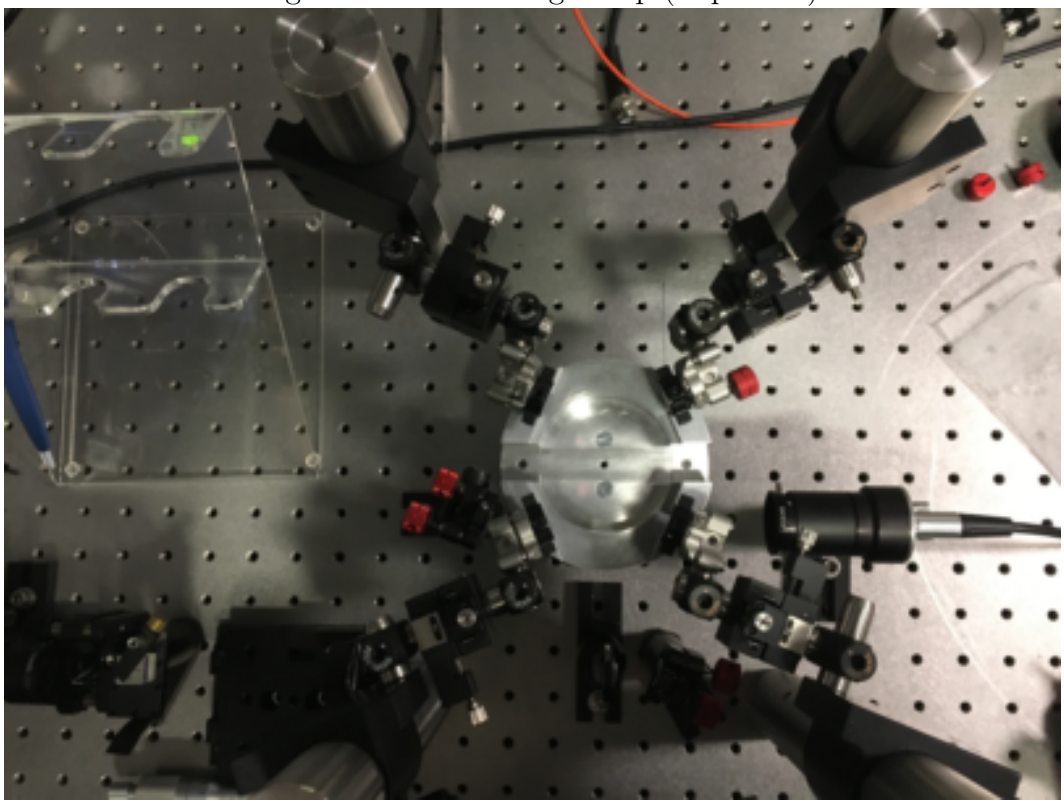

The rest of the alignment process was based on selectively removing degrees of freedom from the setup to ensure there was no unintentional walk-off of the beam in the cavity that would result in cavity twisting. Once the beam line was aligned to the first arm of the guide insert, we no longer touched the input coupling mirrors. We then progressively aligned the mirrors in the cavity along the beam path to ensure the beam passed through all arms of the guide insert. When the alignment was sufficiently close, we began to see cavity resonances on the photodiode. We maximized the cavity resonance signal by making slight changes to the cavity mirror alignment while making sure the beam path adhered to the path dictated by the guide insert. I have included a picture of the setup in the alignment jig in figure 3.12.

Figure 3.12: Mirrors Aligned with Jig

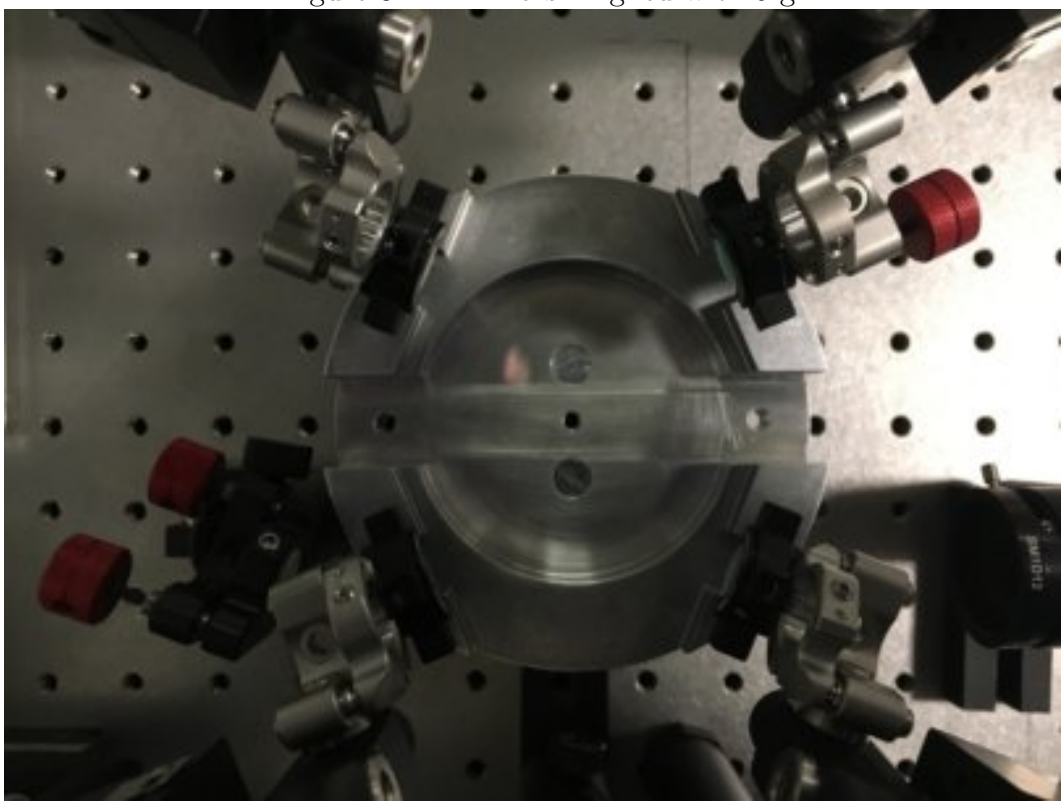

Once the mirrors were aligned properly, we lowered the stage with the jig attached, leaving the mirrors situated in free space. We detached the jig and raised the borosilicate glass spacer on the vertical translation stage up to the height needed to accommodate the pentaprisms. We slid the pentaprisms into position under alignment and bonded them to the mirrors and the substrate using 1.5 μL of 3:1 sodium silicate solution at each bond site. I have included a picture of the setup at this point in figure 3.13. We left the bonds to cure for roughly 2 hours and then detached the mirrors from the mounts and left to cure further for 48 hours.

Figure 3.13: Bowtie During Bonding Process

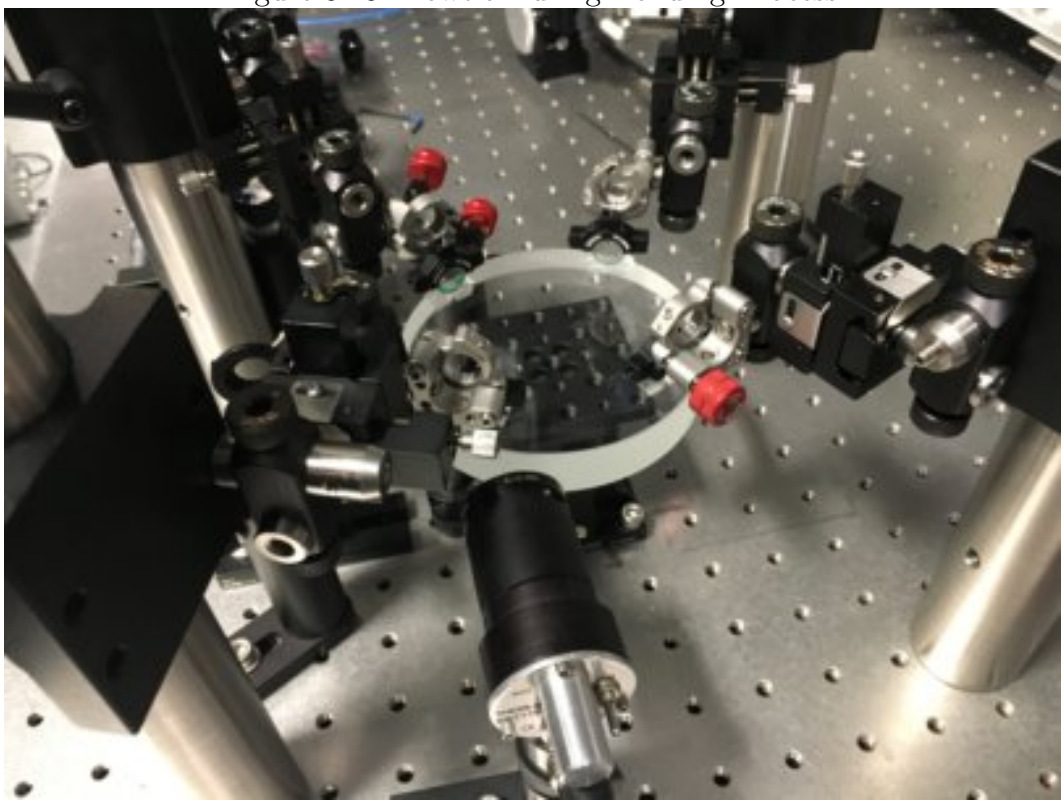

3.2.3 Verification of the Cavity Alignment

I used a 20 MHz modulation signal to measure the FSR and linewidth and calculated the finesse of the cavity. Once again, I measured the parameters for horizontally polarized light, as the vertically polarized light was entirely lost within the cavity. I took the measurements immediately after construction and then a week later to determine the effect of leaving the clean mirrors out in open air. I tabulated the results in table 3.5 It is clear that leaving the mirrors out in open air when making the experimental cavity will present unacceptable losses and line broadening.

Table 3.5: Monolithic Bowtie Prototype

Time	FSR (GHz)	Linewidth (MHz)	Finesse
Right after construction	1.075 ±0.02	2.35 ±0.04	437 ±9
One week after construction	1.075 ±0.02	5.37 ±0.11	200 ±4

I also used a camera to take images of the transmitted beam outside the camera. We observed about 90% of the power was in the TEM_{00} mode. I have shown images of the modes resonating within the cavity in figures 3.14 and 3.15.

Figure 3.14: TEM_{00} mode of the monolithic bowtie cavity

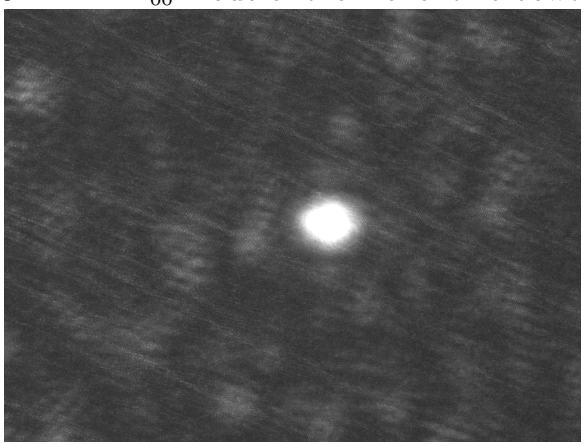

Figure 3.15: Higher order mode of the monolithic bowtie cavity

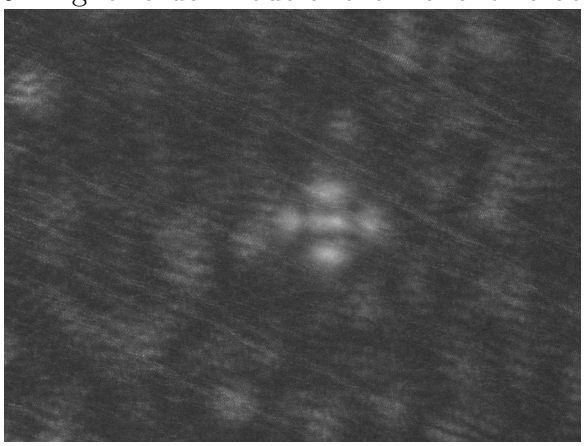

We also checked the cavity twist after bonding to determine the vertical overlap of the two diagonal beams in the cavity. I suspended a sharp (etched tungsten STM) tip in a mechanical 3-axis translation stage and lowered the tip into the cavity beam line. I lowered the tip into one arm of the beam line within 0.5 mm of the point where the beams crossed until I saw a 50% drop in the cavity resonance amplitude. I then translated the tip horizontally out of that beam line arm and into the other and adjusted the vertical alignment until I saw a 50% reduction in the resonance amplitude. I took the difference in vertical positions corresponding to the 50% dropoff as the difference in height of the beams. This technique indicated that one beam was 20 ± 16 μm higher than the other. This figure includes is the uncorrelated combination of all random and systematic errors, including measurement uncertainty of the stage postion, worst-case estimates of non-orthogonality of the translation stages, wedge in the substrate, and variation in thickness of the viton O-rings. Given that the beams are approximately 300 μm in diameter, we judged that the level of twist in the cavity was acceptable for the purpose of trapping.

Estimation of Mirror Losses

While using these mirrors (that were never quoted to be low loss, only highly reflective) we had noticed that we consistently saw relatively low throughput in our cavities, regardless of mode matching or geometry. Using equation 1.17, I determined that, given a finesse of around 200 like we see in all of our monolithic cavities after being out in air for any amount of time, the effective reflectivity of our cavity mirrors is 99.2%. Comparing to the 0.03% measured transmission, we can approximate the scattering coefficient to be about 0.77%. Most of our light that is not reflected is being lost on the cavity mirrors, resulting in low throughput and wider resonances.

Chapter 4

Conclusions

We have seen promising results moving towards building the experimental cavity. We have verified that the hydroxide catalysis bonded cavities can withstand moderate bakeout temperatures and can sit in a vacuum chamber without large amounts of outgassing. We have also developed a set of alignment procedures and jigs for aligning bowtie cavities in free space and bonding them to a flat substrate.

While we do not yet have the experimental monolithic bowtie cavity constructed, that step seems just around the corner. We chose not to construct it at the last minute to avoid user error due to rushing and to perform further analysis on our existing cavities. The experimental cavity will be introduced into an ultra-clean system where in-situ adjustment or correction is impossible, and risks of contamination are unacceptable if they will disrupt the rest of the experiment. We need to get it right the first time, and so we chose to play it safe.

To that end, some of the next few steps will include vacuum testing the prototype bowtie and bringing it down to pressures we are likely to see in experiment, i.e. below 10^{-11} Torr. With the introduction of more bonding material in the bowtie compared

to the linear due to more bonds being used, it is possible the bowtie will introduce either more water vapor or more room contaminants or both into the chamber. A bakeout stress test to push the limits of the maximum temperature and differential expansion due to temperature the bonds can withstand might also be a good idea.

While most of the monolithic bowtie alignment process seemed to work as planned, during alignment I noticed that the widths of the grooves used as beam guides in the alignment jig insert seemed overly forgiving. We were initially concerned that narrower guides might result in clipping that brought high losses, but we did not observe any such phenomenon, and reducing the diameter of the alingment grooves might give us tighter tolerances on cavity twist. We could also slot in a pellicle into the alignment jig, which is a thin screen that shows beam lines that might indicate degree of beam overlap inside the cavity during the alignment process. The bowtie cavity with the Thorlabs mirrors did not provide high enough intracavity power to observe spots on the pellicle, but the power will be much higher in the low loss cavity we will build and might allow for its use. Additionally, future efforts to measure the vertical offset of the cavity beams should try to remove possible sources systematic error, for example by establishing tighter bounds on non-orthogonality and mechanical runout, and by using a four-point measurement.

Appendix A

Part Numbers

Table A.1: Part Numbers

PDH Locking Equipment	
1 MHz EOM	Thorlabs E0-PM-NR-C2
Locking Servo	New Focus LB1005
Mixer	MiniCircuits ZAD-8+
Input Amplifier	MiniCircuits ZX60-100VHX
Laser Piezo Controller	Thorlabs MDT6984B
EOM Amplifier	Thorlabs HVA200
Transmitted Beam Photodiode	Thorlabs PDA10C
Reflected Beam Photodiode	Thorlabs PDA10CS
Lasers	
780 nm Laser	New Focus Velocity 6312
780 nm Laser (Higher Power)	Toptica DLX 110
1068 nm Laser	Koheras Boostik Fiber Laser

Appendix B

mode matching Procedure

To modematch an incoming beam to a cavity, the problem can be reframed to be to match the incoming beam's Rayleigh Length to that of the cavity mode's and then to position the beam optics so that the location of the beam waist of the input beam coincides with position of the beam waist of the cavity mode inside the cavity.

For the sake of simplicity, I'll show the procedure only for mode matching to a linear cavity, but mode matching to a bowtie cavity uses a similar procedure that involves more ray matrices due to there being more cavity mirrors. I describe the theoretical underpinnings referenced in this section in 1.2.3.

The first step is to determine the beam modes both outside and inside the cavity. The beam mode inside the cavity can be modeled using ray matrices, where we assume an incoming beam travels one cavity length inside the cavity, reflects off a cavity mirror, then travels the same distance inside the cavity and reflects off of the other cavity mirror. The ray matrix representation of a beam traveling through space is given by

$$S = \begin{bmatrix} 1 & L \\ 0 & 1 \end{bmatrix} \tag{B.1}$$

and for reflecting off of a mirror with radius of curvature R the representation is

$$M = \begin{bmatrix} 1 & 0 \\ -2/R & 1 \end{bmatrix} \tag{B.2}$$

and so the ray matrix for a cavity is the product of

$$CAV = \begin{bmatrix} 1 & 0 \\ -2/R & 1 \end{bmatrix} \begin{bmatrix} 1 & L \\ 0 & 1 \end{bmatrix} \begin{bmatrix} 1 & 0 \\ -2/R & 1 \end{bmatrix} \begin{bmatrix} 1 & L \\ 0 & 1 \end{bmatrix} \tag{B.3}$$

Recall that the q parameter evolves with under a ray matrix under the transformation

$$q_2(z) = \frac{Aq_1(z) + B}{Cq_1(z) + D} \tag{B.4}$$

For the cavity to be stable, rays must trace back onto themselves on return trips, so we can impose on our system that for return trips, $q_2 = q_1$. Solving the above equation under this condition gives an equation for the q parameter in terms of the cavity ray matrix ABCD parameters.

$$Cq^2 + (D - A)q - B = 0 \tag{B.5}$$

Solving the above equation for q gives us the q parameter for the cavity.

Outside the cavity, the q parameter can simply be measured using a camera to

measure the beam $\frac{1}{e^2}$ radius at points along the beam line. Finding the location and size of the beam waist outside the camera fixes the q parameter, such that if the Rayleigh Length is

$$z_0 = \frac{\pi w_0^2}{\lambda} \tag{B.6}$$

then the q parameter is

$$q(z) = z + iz_0 \tag{B.7}$$

where z is the position from the waist along the beam line. Assuming now that we start at some position z along the beam line, using a lens pair we are able to match the Rayleigh Length of the incoming beam with that of the cavity. The ray transfer matrix for a pair of lenses with focal lengths f_1 and f_2 separated by a distance d apart at a distance z from the initial beam waist is

$$X = \begin{bmatrix} 1 & 0 \\ -1/f_2 & 1 \end{bmatrix} \begin{bmatrix} 1 & L \\ 0 & 1 \end{bmatrix} \begin{bmatrix} 1 & 0 \\ -1/f_1 & 1 \end{bmatrix} \begin{bmatrix} 1 & L \\ 0 & 1 \end{bmatrix} \tag{B.8}$$

By solving for the imaginary part of the new q parameter and picking the lens focal lengths and spacings correctly, you can match the waist size to that of the cavity waist size. The real part of the new q parameter is the distance between the second lens and the new waist. All that is needed to finish mode matching at this point is to shift relative positions of the external beam lenses and the cavity until their waists overlap.

Bibliography

[1] J. Alnis, A. Matveev, N. Kolachevsky, Th. Udem, and T. W. Hänsch, *Subhertz linewidth diode lasers by stabilization to vibrationally and thermally compensated ultralow-expansion glass fabry-pérot cavities*, Phys. Rev. A **77** (2008), 053809.

[2] Simon Bernon, *Trapping and nondemolition measurement of cold atoms in a high-finesse ring cavity*, Ph.D. thesis, 2011.

[3] A. Bertoldi, S. Bernon, T. Vanderbruggen, A. Landragin, and P. Bouyer, *In situ characterization of an optical cavity using atomic light shift*, Opt. Lett. **35** (2010), no. 22, 3769–3771.

[4] Eric D. Black, *An introduction to pounddreverhall laser frequency stabilization*, American Journal of Physics **69** (2001), no. 1, 79–87.

[5] Cheng Chin, Rudolf Grimm, Paul Julienne, and Eite Tiesinga, *Feshbach resonances in ultracold gases*, Rev. Mod. Phys. **82** (2010), 1225–1286.

[6] Jean Dalibard, Fabrice Gerbier, Gediminas Juzeliūnas, and Patrik Öhberg, *Colloquium : Artificial gauge potentials for neutral atoms*, Rev. Mod. Phys. **83** (2011), 1523–1543.

[7] Peter Domokos and Helmut Ritsch, *Collective Cooling and Self-Organization of Atoms in a Cavity*, Physical Review Letters **89** (2002), no. 25, 253003.

[8] E J Elliffe, J. Bogenstahl, A. Deshpande, J. Hough, C. Killow, S. Reid, D. Robertson, S. Rowan, H. Ward, and G. Cagnoli, *Hydroxide-catalysis bonding for stable optical systems for space*, Classical and Quantum Gravity **22** (2005), no. 10, S257–S267.

[9] Simin Feng and Herbert G. Winful, *Physical origin of the gouy phase shift*, 2000.

[10] Rudolf Grimm, Matthias Weidemller, and Yurii B. Ovchinnikov, *Optical dipole traps for neutral atoms*, Advances In Atomic, Molecular, and Optical Physics, vol. 42, Academic Press, 2000, pp. 95 – 170.

[11] A.K. Gupta, K.V. Kurup (Smt), J Santhanam, and P Vijendran, *Outgassing from epoxy resins and methods for its reduction*, Vacuum **27** (1977), no. 2, 61 – 63.

[12] D. Kruse, M. Ruder, J. Benhelm, C. von Cube, C. Zimmermann, Ph. W. Courteille, Th. Elsässer, B. Nagorny, and A. Hemmerich, *Cold atoms in a high-q ring cavity*, Phys. Rev. A **67** (2003), 051802.

[13] Y. Matsuda and H. Shimahara, *Fulde-Ferrell-Larkin-Ovchinnikov State in Heavy Fermion Superconductors*, Journal of the Physical Society of Japan **76** (2007), no. 5, 051005.

[14] A. Mosk, S. Jochim, H. Moritz, Th. Elsässer, M. Weidemüller, and R. Grimm, *Resonator-enhanced optical dipole trap for fermionic lithium atoms*, Opt. Lett. **26** (2001), no. 23, 1837–1839.

[15] Mohit Randeria and Edward Taylor, *Crossover from bardeen-cooper-schrieffer to bose-einstein condensation and the unitary fermi gas*, Annual Review of Condensed Matter Physics **5** (2014), no. 1, 209–232.

[16] Helmut Ritsch, Peter Domokos, Ferdinand Brennecke, and Tilman Esslinger, *Cold atoms in cavity-generated dynamical optical potentials*, Rev. Mod. Phys. **85** (2013), 553–601.

[17] Bahaa E. A. Saleh and Malvin Carl Teich, *Principles of photonics*, 5 ed., John Wiley & Sons, Inc, 1991.

[18] Florian Schreck, *Mixtures of Ultracold Gases: Fermia Sea and Bose-Einstein Condensate of Lithium Isotopes*, Ph.D. thesis, 2002.

[19] Bruno Zimmermann, *Microscopy of Ultra-Cold Fermionic Lithium*, (2010), no. 19085, 136.

[20] Martin Zwierlein, *High-temperature superfluidity in an ultracold fermi gas*, Ph.D. thesis, 2006.

Acknowledgements

I would like to thank my advisor Kevin Wright for being an endless font of knowledge of all things experimental physics and for guiding me through my time in graduate school. I'd also like to thank Sarah Khatry for her prior work on this project and Yanping Cai and Dan Allman for editing and being excellent labmates. I would also like to thank Dwayne Adams for his excellent machining work on this project.

Last and certainly not least I'd like to thank my mom, dad, and sister (hi Jay) for being loving and supportive.